JOURNAL OF GEOPHYSICAL RESEARCH, VOL. 113, D00C17, doi:10.1029/2008JD010077, 2008

Click Here for Full Article

Overview of the Dust and Biomass-burning Experiment and African Monsoon Multidisciplinary Analysis Special Observing Period-0

J. M. Haywood,[1] J. Pelon,[2] P. Formenti,[3] N. Bharmal,[4] M. Brooks,[1] G. Capes,[5] P. Chazette,[6] C. Chou,[3] S. Christopher,[7] H. Coe,[5] J. Cuesta,[8] Y. Derimian,[9] K. Desboeufs,[3] G. Greed,[1] M. Harrison,[1] B. Heese,[10] E. J. Highwood,[11] B. Johnson,[1] M. Mallet,[12] B. Marticorena,[3] J. Marsham,[13] S. Milton,[1] G. Myhre,[14] S. R. Osborne,[1] D. J. Parker,[13] J.-L. Rajot,[15] M. Schulz,[6] A. Slingo,[4,16] D. Tanré,[9] and P. Tulet[17]

Received 6 March 2008; revised 30 June 2008; accepted 22 August 2008; published 9 December 2008.

[1] The African Monsoon Multidisciplinary Analysis (AMMA) is a major international campaign investigating far-reaching aspects of the African monsoon, climate and the hydrological cycle. A special observing period was established for the dry season (SOP0) with a focus on aerosol and radiation measurements. SOP0 took place during January and February 2006 and involved several ground-based measurement sites across west Africa. These were augmented by aircraft measurements made by the Facility for Airborne Atmospheric Measurements (FAAM) aircraft during the Dust and Biomass-burning Experiment (DABEX), measurements from an ultralight aircraft, and dedicated modeling efforts. We provide an overview of these measurement and modeling studies together with an analysis of the meteorological conditions that determined the aerosol transport and link the results together to provide a balanced synthesis. The biomass burning aerosol was significantly more absorbing than that measured in other areas and, unlike industrial areas, the ratio of excess carbon monoxide to organic carbon was invariant, which may be owing to interaction between the organic carbon and mineral dust aerosol. The mineral dust aerosol in situ filter measurements close to Niamey reveals very little absorption, while other measurements and remote sensing inversions suggest significantly more absorption. The influence of both mineral dust and biomass burning aerosol on the radiation budget is significant throughout the period, implying that meteorological models should include their radiative effects for accurate weather forecasts and climate simulations. Generally, the operational meteorological models that simulate the production and transport of mineral dust show skill at lead times of 5 days or more. Climate models that need to accurately simulate the vertical profiles of both anthropogenic and natural aerosols to accurately represent the direct and indirect effects of aerosols appear to do a reasonable job, although the magnitude of the aerosol scattering is strongly dependent upon the emission data set.

Citation: Haywood, J. M., et al. (2008), Overview of the Dust and Biomass-burning Experiment and African Monsoon Multidisciplinary Analysis Special Observing Period-0, *J. Geophys. Res.*, *113*, D00C17, doi:10.1029/2008JD010077.

[1]Met Office, Exeter, UK.
[2]Service de Aéronomie, IPSL, Université Pierre et Marie Curie, Paris, France.
[3]LISA, CNRS, France.
[4]ESSC, University of Reading, Reading, UK.
[5]School of Earth, Atmospheric and Environmental Sciences, University of Manchester, Manchester, UK.
[6]CEA, DSM, LSCE, Gif sur Yvette, France.
[7]Earth System Science Center, NSSTC, University of Alabama, Huntsville, Alabama, USA.
[8]Laboratoire de Météorologie Dynamique, Institute Pierre Simon Laplace, Ecole Polytechnique, Palaiseau, France.
[9]Laboratoire d'Optique Atmosphérique, Université des Sciences et Technologies de Lille, CNRS, Villeneuve d'Ascq, France.
[10]Leibniz Institute for Tropospheric Research, Leipzig, Germany.
[11]Department of Meteorology, University of Reading, Reading, UK.
[12]Laboratoire d'Aerologie, UPS, CNRS, UMR5560, Toulouse, France.
[13]Institute for Climate and Atmospheric Science Environment, School of Earth and Environment, University of Leeds, Leeds, UK.
[14]Center for International Climate and Environmental Research, Oslo, Norway.
[15]IRD, UR 176, Niamey, Niger.
[16]Deceased 14 October 2008.
[17]CNRM, GAME, Meteo-France, Toulouse, France.

Copyright 2008 by the American Geophysical Union.
0148-0227/08/2008JD010077$09.00

1. Introduction

[2] Aerosols have a significant influence upon the radiation balance of the planet at local, regional and global scales [e.g., *Haywood and Boucher*, 2000]. These aerosols may be of primarily natural origin (e.g., sea salt, biogenic or mineral dust aerosols), or of primarily anthropogenic origin (e.g., sulphate, nitrate, black carbon or biomass burning smoke aerosols) [e.g., *Forster et al.*, 2007]. The Sahara desert in West Africa is the largest desert and acts as the strongest source of mineral dust aerosol in the world [e.g., *Woodward*, 2001]. In addition, the burning of agricultural waste in the Sahelian region during the dry season means that West Africa is a strong source of biomass burning smoke aerosol [e.g., *Bond et al.*, 2004] from anthropogenic activities. Indeed, the contribution to biomass burning smoke over West Africa from naturally occurring fires caused by, for example, lightening strikes is insignificant at this time of the year [e.g., *Christian et al.*, 2003], so the biomass burning aerosol can be considered to be of anthropogenic origin. Both mineral dust and biomass burning aerosols scatter and absorb solar radiation, while mineral dust aerosols are of sufficiently large size to interact with terrestrial radiation [e.g., *Forster et al.*, 2007]. The pattern of biomass burning emissions in Africa follows a well determined seasonal cycle related to precipitation associated with the seasonal shift in the Inter-Tropical Convergence Zone (ITCZ) [e.g., *Swap et al.*, 2002]. Thus maximum emissions of biomass burning aerosol from the sub-Sahelian regions of northern Africa occur during December–February with very little open biomass burning occurring during August–November. A map of the fire activity as detected from the MODIS sensor for 2006 over the African continent is shown in Figure 1 which clearly shows the significant influence of biomass burning during January 2006 compared with other months. Mineral dust is emitted from North Africa throughout the year and thus in December–February the interaction of mineral dust and biomass burning aerosols is at a maximum.

[3] Previous major measurement campaigns have investigated the physical and radiative properties of biomass burning aerosols and mineral dust (frequently in conjunction with other aerosol types, such as industrial pollution) as summarized in Table 1.

[4] Furthermore, although source regions for dust and biomass burning particles can be identified by radiometry from satellite, one of the main difficulties remains in precisely identifying the transport and modification/interaction processes acting on particles in west Africa, which is critical for better quantification of aerosol radiative impact at the regional scale. Until now, no large-scale multinational campaign has specifically investigated the roles of mineral dust and biomass burning aerosol in West Africa and their influence on the radiation balance of the Earth/atmosphere system. The AMMA campaign is a major international project to improve our understanding of the monsoon and the meteorology and climatology of West Africa and the associated impacts on issues of health, water resources, and food security [*Redelsperger et al.*, 2006]. The observational strategy identified three nested observational periods: (1) Long-Term Observing Period (LOP) which incorporates the historical observations and additional long-term observations over the period 2002–2010; (2) Enhanced Observing Period (EOP) which involves enhanced observational capabilities over the period 2005–2007; and (3) Special Observing Period (SOP) which focuses on 4 specific periods: SOP0, the dry season (January–February 2006); SOP1, monsoon onset (May–June 2006); SOP2 monsoon (July–August 2006); SOP3 monsoon decay (August–September 2006). The Dust and Biomass burning Experiment (DABEX) was a complementary study by the UK Met Office with the FAAM BAe146 aircraft which was coordinated to coincide with the AMMA SOP0.

[5] The primary aims of both AMMA SOP0 and DABEX were: (1) to perform high-quality in situ and remote sensing measurements of the optical and physical properties of biomass burning aerosols from West Africa; (2) to perform high-quality in situ and remote sensing measurements of the optical and physical properties of natural mineral dust aerosols over West Africa; (3) to determine the interaction between the anthropogenic biomass burning aerosols and natural mineral dust aerosols using a combination of chemical, physical and optical measurements; (4) to provide high-quality spectral measurements of the solar and terrestrial radiative effects of both biomass burning aerosol and mineral dust aerosol; (5) to determine the consistency between in situ measurements/satellite and surface based remote sensing methods of the effects on the radiation budget of the Earth of the composite biomass and mineral dust aerosols; and (6) to model the effect of the biomass and mineral dust aerosols on a regional and global scale and estimate the impact on the global radiation balance of the Earth/Atmosphere system.

[6] The U.S. Department of Energy's Atmospheric Radiation Measurements (ARM) Program Mobile Facility (AMF) was fully equipped with comprehensive instrumentation and was located at Niamey airport [*Miller and Slingo*, 2007] under the Radiative Atmospheric Divergence using AMF, GERB data and AMMA STations (RADAGAST) project. The prime objective of RADAGAST was to combine measurements of the top of the atmosphere radiation balance with high-quality measurements at the surface to estimate the divergence of shortwave and longwave energy through the atmosphere. The AMF operated in Niamey throughout 2006, and a related AMF ancillary site including a limited number of passive radiation sensors was established at Banizoumbou. The AMF data therefore provide complementary measurements to those made at other AMMA sites. A full description of the seasonal cycle of the meteorology of the region observed by the AMF is provided by *Slingo et al.* [2008].

[7] One further measurement campaign in West Africa during 2006 is worthy of note: the Dust Outflow and Deposition to the Ocean (DODO), during which the FAAM aircraft was based in Dakar for two periods during February and August 2006 immediately subsequent to the DABEX and AMMA SOP2 deployments. During DODO1, the BAe146 performed a total of seven flights totaling approximately 29hours of flying during the period 7–16 February. *McConnell et al.* [2008] provide details of the flights and findings for DODO1. During DODO2 six flights totaling approximately 26.5hours were performed from Dakar during the period 21–29 August. These flights were mainly

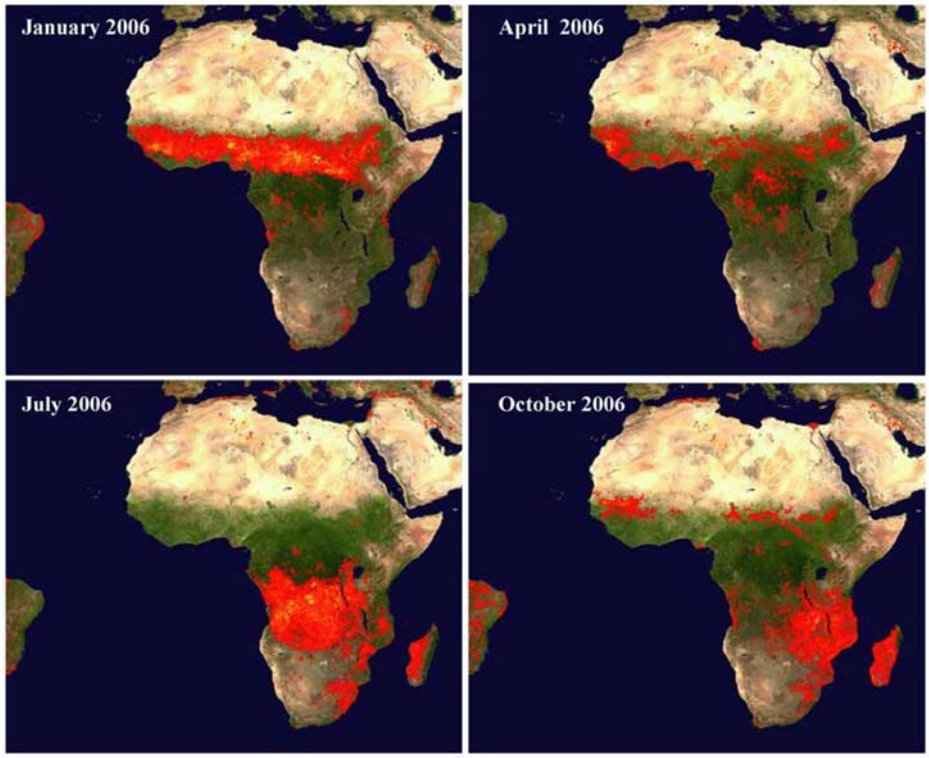

Figure 1. MODIS fire retrievals showing the seasonality of biomass burning over the African continent during 2006. Images show 10-day mean midmonth composites in each case. Image courtesy of MODIS Rapid Response Project at NASA/GSFC (http://rapidfire.sci.gsfc.nasa.gov/firemaps/).

performed over ocean, but some flights were made over land in areas of high dust loadings [e.g., *Greed et al.*, 2008].

[8] A summary of the various campaigns and their duration is presented in Figure 2.

[9] This overview paper primarily summarizes the measurement and modeling efforts during the dry season (SOP0), although some of the measurements and modeling studies are of longer duration or outside of this time period. However, all of the studies presented here have aerosol horizontal and vertical spatial distributions, their physical and optical properties, and their effect on the radiation budget as their primary focus. Section 2 describes the surface based observational sites and the measurements made and section 3 describes the instrumentation and flight patterns of the two aircraft involved with the study. Section 4 provides an overview of the meteorological conditions experienced over west Africa during the period, with an emphasis on the meteorological variables that are important in determining aerosol transport. Section 5 provides an overview of the aerosol chemical, physical and optical properties and the effects of these aerosols on atmospheric radiation. Modeling and satellite instrumental studies are discussed in section 6 before conclusions are presented in section 7.

2. Overview of the Surface Observation Network

[10] A wide observational network was established for AMMA SOP0. The surface sites ranged from surface Sun photometers that are installed on a semipermanent basis

Table 1. A Summary of Major Measurement Campaigns Focusing on Mineral Dust and Biomass Burning During the Past Decade[a]

Aerosol Type	Study	Area	Reference
Biomass burning aerosol	SCAR-B	South America/Brazil	*Kaufman et al.* [1998]
	INDOEX	India/Indian Ocean	*Ramanathan et al.* [2001]
	SAFARI-2000	South Africa	*Swap et al.* [2002]
	SMOCC	South America/Brazil	*Andreae et al.* [2004]
Mineral dust	ACE-2	Tenerife	*Raes et al.* [2000]
	SHADE	West Africa	*Tanré et al.* [2003]
	MINOS	Mediterranean	*Lelieveld et al.* [2002]
	ACE-ASIA	East Asia	*Huebert et al.* [2003]
	PRIDE	Puerto Rico	*Reid et al.* [2003]
	BODEX	Chad	*Washington et al.* [2006]
	DODO	West Africa	*McConnell et al.* [2008]

[a]The reader is referred to the individual references for the meaning of the acronyms.

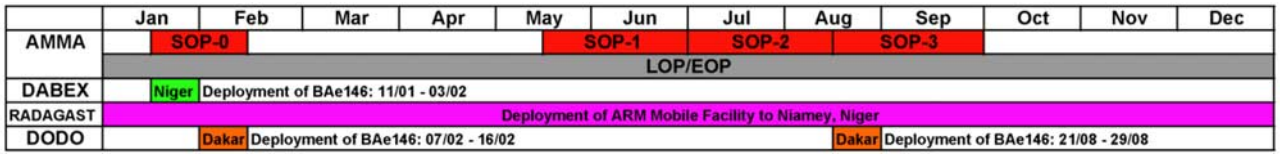

Figure 2. Calendar showing the duration of the deployment of AMMA Special Observing Periods, Extended Observing Periods, and Long-Term Observing Periods (SOPs, EOPs, and LOPs), DABEX, RADAGAST, and DODO deployments.

as part of the Aerosol Robotic Network (AERONET) and its French counterpart PHOtométrie pour le Traitement Opérationnel de Normalization Satellitaire (PHOTONS, http://www-loa.univ-lille1.fr/photons), to specific fully instrumented sites that made in situ and remote sensing measurements. Four fully equipped ground-based stations (super sites) were established: Banizoumbou (Niger), Djougou (Benin), M'Bour (Senegal) and Tamanrasset (Algeria), all coinciding with AERONET/PHOTONS stations, provided high-quality and high-frequency aerosol and radiation measurements. Measurements include a complete set of physicochemical and optical measurements, including size-segregated sampling for chemical and mineralogical analysis, measurements of number size distributions, spectral scattering and absorption coefficients, aerosol vertical profiles, column-integrated content and properties, as well as spectral and/or broadband radiation fluxes. Some of the stations (Agoufou, Banizoumbou, Djougou) are also part of the IDAF/DEBITS network installed in the tropics as part of IGBP program for the analysis of atmospheric composition (http://medias.obs-mip.fr/idaf). The geographic location of some of the sites discussed here is shown in Figure 3 and the measurements made are shown in Table 2.

[11] The location of the four AMMA super stations was chosen to cover a large spatial domain to investigate the variability of the aerosol load in western Africa: two stations (Banizoumbou, Tamanrasset) were located in areas expected to be dominated by mineral dust and two (Djougou, M'Bour) in areas expected to have a large contribution from biomass burning aerosols. In addition to standard meteorological measurements, the AMMA super sites at Banizoumbou, Djougou, Tamanrasset, and M'Bour were fully equipped with aerosol, chemistry and atmospheric radiation equipment, details of which are summarized in Table 3 (see *Rajot et al.* [2008], *Mallet et al.* [2008], *Cuesta et al.* [2008], and *Derimian et al.* [2008] for full details). In addition, the radiosonde network was enhanced to provide a more comprehensive network throughout the AMMA EOP [*Parker et al.*, 2008].

3. Overview of the Aircraft Capability and Operations

[12] During DABEX/AMMA SOP0 two very different aircraft were deployed to Niamey, Niger; the FAAM BAe146 and an ultralight aircraft (ULA). Photographs of these aircraft are shown in Figure 4. Here we describe the

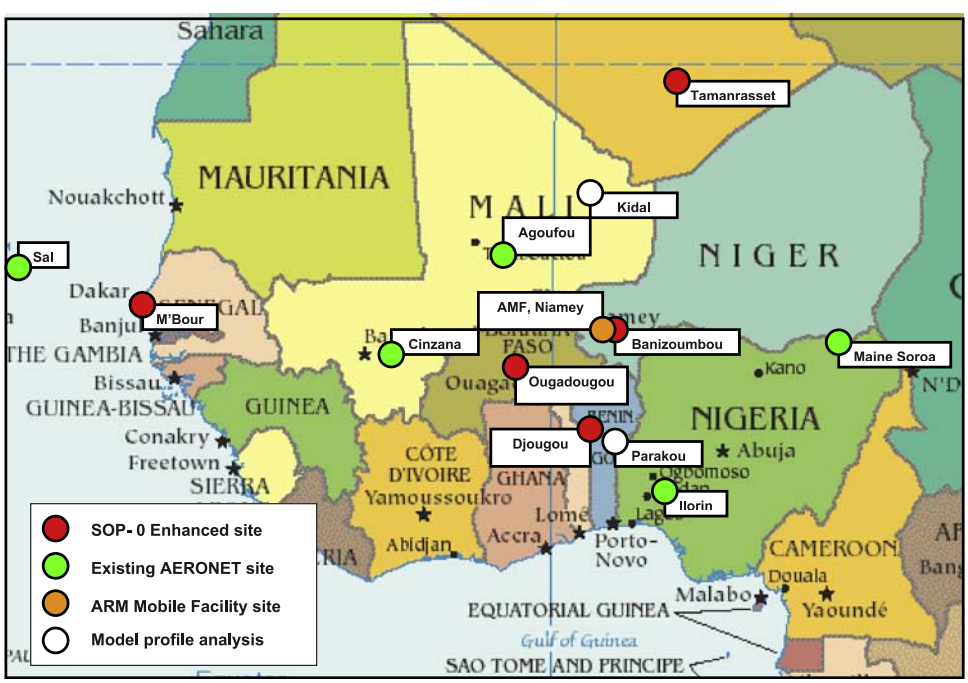

Figure 3. Showing the position of the enhanced sites during AMMA SOP0. The "model profile analysis" sites are indicated (section 4).

Table 2. Description of the Instrumentation Installed at the Various Surface-Based Sites During DABEX/AMMA SOP0[a]

Site	Designation	Location	Instrumentation					References
			Sunphoto	SW BBR	LW BBR	Lidar	Aerosol	
Niamey Airport	ARM Mobile Facility	Niger (13.5°N, 2.2°E)	MT, MFRSR	KZ	E	β + R	P, C	*Miller and Slingo* [2007]
Banizoumbou	AMMA SS, AMF Ancillary	Niger (13.5°N, 2.7°E)	C-A (P) MFRSR	KZ	E	β + R	P, C	*Rajot et al.* [2008], *Heese and Wiegner* [2008]
Djougou	AMMA SS	Benin (9.7°N, 1.6°E)	C-A (P)	KZ	NI	β	P, C	*Mallet et al.* [2008], *Pelon et al.* [2008]
Ilorin	AERONET	Nigeria (8.3°N, 4.34°E)	C-A	NI	NI	β	NI	*Nwofor et al.* [2007]
M'Bour	AMMA SS	Senegal (14.4°N, 16.9°W)	C-A (P)	KZ	E	β	P, C	*Derimian et al.* [2008]
Tamanrasset	AMMA SS	Algeria (22.8°N, 5.5°E)	C-A (P)	KZ	E	β	P, C	*Cuesta et al.* [2008]
Agoufou	AERONET	Mali (15.3°N, 1.4°W)	C-A (P)	NI	NI	NI	NI	http://aeronet.gsfc.nasa.gov and http://loaphotons.univ_lille1.fr/photons/
Cinzana	AERONET	Mali (13.3°N, 5.9°W)	C-A (P)	NI	NI	NI	NI	http://aeronet.gsfc.nasa.gov and http://loaphotons.univ-lille1.fr/photons/
Maine-Soroa	AERONET	Niger (13,2°N, 12°W)	C-A	NI	NI	NI	NI	http://aeronet.gsfc.nasa.gov

[a]Designation: ARM, (Atmospheric Radiation Measurements) Mobile Facility; AMMA SS denotes AMMA super site. Sunphoto denotes Sun photometer: Microtops II, MT; Multifilter Rotating shadow-band radiometer, MFRSR; CIMELS AERONET, C-A; part of the PHOTONS network (http://loaphotons.univ-lille1.fr/photons/), C-A (P). SW BBR denotes shortwave broadband radiometer: Kipp and Zonen, KZ; long-wave broadband radiometer, LW BBR. Lidar: backscatter, β; Raman, R. Aerosol: physics, P; chemistry, C. NI denotes not installed.

scientific payload of each of the aircraft and the flight patterns performed.

3.1. FAAM BAe146

[13] The FAAM BAe146 is jointly funded by the Met Office and the Natural Environment Research Council (NERC) and has the largest payload of the European fleet of meteorological research aircraft. The aircraft is capable of carrying 2 crew, 18 scientists and a total scientific payload of up to 4000 kg for a distance of 3700 km with a ceiling of 35,000 feet and has a typical science speed of 110 m s^{-1}. The endurance of the BAe146 aircraft is typically up to 6 h depending on the scientific payload, the flight patterns, ambient meteorological conditions and the proximity of diversion airports. During DABEX the maximum duration of the flights was around 4.75 h.

[14] The scientific payload was tailored for aerosol, radiation, and basic gas phase chemistry measurements, as well as measurements of standard meteorological variables such as temperature, humidity, and wind speed and direction. A summary of the dedicated measurement equipment is provided in Table 4 (full details available at http://www.faam.ac.uk/).

[15] The BAe146 flew a total of 13 dedicated scientific flights for a total of approximately 55 h. The flight tracks of the aircraft are shown in Figure 5 which shows 4 local flights, 6 flights to the south of Niamey into Benin and Nigeria to probe the biomass burning plumes either as fresh plumes or in conjunction with the surface/AERONET sites of Banizoumbou, Djougou, and Ilorin [e.g., *Johnson et al.*, 2008a; *Capes et al.*, 2008; *Mallet et al.*, 2008], and 3 flights to the northeast to probe the mineral dust plume [e.g., *Osborne et al.*, 2008; *Chou et al.*, 2008; *Formenti et al.*, 2008].

3.2. Ultralight Aircraft

[16] The ULA has a science payload of 120 kg, a ceiling of around 19,000 feet, and endurance of up to 3 h in the African environment. The ULA was equipped with a pointable Lidar Aérosols UltraViolet Aéroporté (LAUVA) UV backscatter lidar which operates at a wavelength of 355 nm, a Vaisala PTU200 meteorological probe to measure temperature, pressure and relative humidity, and a lightweight nephelometer-type instrument which works at a wavelength of 870 nm [*Chazette et al.*, 2007; *Dulac et al.*, 2001].

[17] The relatively slow airspeed (20–22 m s^{-1}) of the ULA means that it is ideal for making intensive measurements in a small column of atmosphere. Thirteen scientific flights were performed during the period 24 January until 1 February 2006. These flights included 3 profiles at Niamey coincident with the BAe146 operations, two flights to Banizoumbou with descents over the Banizoumbou site, and 2 N–S transects to La Tapoa some 110 km to the south of Niamey airport. The approximate operating area of the ULA is shown in Figure 5. When the ULA was not flying the lidar was frequently operated as a surface based platform at Niamey airport, which provides very useful information upon the time evolution of aerosol (see section 4).

4. Overview of Meteorological Conditions Affecting Aerosol Transport

[18] The meteorological conditions in West Africa show tremendous variability throughout the year. *Slingo et al.* [2008] provide a summary of surface and profile data from the AMF stationed in Niamey, Niger throughout 2006, and *Rajot et al.* [2008] provide complementary surface measurements from the Banizoumbou super site with more emphasis on aerosol variability associated with the prevailing meteorology. *Cuesta et al.* [2008] present profile and surface based measurements of the meteorological conditions throughout 2006 at the remote Tamanrasset site in southern Algeria.

[19] *Derimian et al.* [2008] provide an analysis of MODIS aerosol optical depths for the January–February period for 2001–2006, and show that the biomass burning aerosol optical depth was rather weak compared to other years presumably because of reduced emissions. Here, we discuss the meteorological conditions over the observational

Table 3. Description of the Relevant Instruments Installed at the AMMA SOP-0 Super Sites for Deriving the Aerosol Physical, Chemical, and Optical Properties, the Gas Phase Chemistry, and Atmospheric Radiation[a]

	Djougou		Banizoumbou		M'Bour		Tamanrasset	
	Instruments	Frequency	Instruments	Frequency	Instruments	Frequency	Instruments	Frequency
Aerosol phys/chem/optical properties	1 CPC (0.01–3 μm)	continuous			1 CPC (0.05–1 μm)	continuous		
Number concentration					1 Laser OPC (0.3–5.0 μm)	continuous		
CCN concentration	CCN counter	continuous						
Mass concentration			1 TEOM (TSP IPC) 1 TEOM (PM10)	continuous continuous	1 TEOM (PM10)	continuous		
Number size distribution	1 GRIMM OPC (0.3–20 μm) 1 SMPS (3–300 nm)	continuous continuous	2 GRIMM OPC (0.3–20 μm, IPC)	continuous	1 Laser OPC (0.3–5.0 μm)	continuous	1 GRIMM OPC (0.3–20 μm)	continuous
Mass size concentration and composition	2 cascade impactors (13 stages)	1/day	2 cascade impactors (4 and 13 stages)	1/day + events	1 cascade impactor (4 stages)	1/day + event		
Elemental composition	PM 2.5/10 + bulk filtration lines	1–2/day	bulk filtration lines (IPC) + 1 P.M.10	2/day + events	bulk filtration lines (IPC/PM10)	1/day + event	PM 20; PM 10; PM 2.5; PM 1	1/day
Mineralogy + carbon fraction	PM 2.5/10 + bulk filtration lines	1–2/day	bulk filtration lines (IPC)	2/day + events	dry deposition sampler			
Shape and composition of individual particles			bulk filtration lines (IPC)	2/day	4-stage cascade impactor	1/day + event	bulk filtration lines (PM10)	event
Water-soluble fraction, Fe speciation	PM 2.5/10 filtration lines	1/week	bulk filtration lines (IPC)	1/day	bulk filtration lines (IPC/PM10)	1/day + event		
Isotopic iron composition					bulk filtration line (IPC/PM10)	1/day		
Vertical profile	1 micro-lidar	continuous	1 lidar (depol/N2 Raman)	continuous	1 lidar	continuous	1 miniLidar (multiλ elastic and Raman channels backscatter)	continuous
	1 lidar ceilometer	continuous	1 micro-lidar	(twice daytime/ nighttime)	1 micro-lidar	nighttime		
Column optical properties	AERONET	continuous	AERONET	continuous	AERONET	continuous	TReSS sunphotometer	continuous
Scattering coefficient	1 nephelometer (1-λ)	continuous	1 nephelometer (3-λ) (IPC)	continuous	1 nephelometer (1-λ)	continuous	1 scatterometer (1-λ)	continuous
Absorption coefficient	1 aethalometer (7-λ)	continuous	1 aethalometer (7-λ) (IPC)	continuous	1 aethalometer (7-λ)	continuous		
Gas phase chemistry: O_3, CO, SO_2, NO_x, COV	active sampler (real time monitoring)	continuous	analyzer in real-time monitoring	continuous			1 Dobson	continuous
Radiation: VIS, IR	4 component radiometers	continuous	1 pyranometer (0.3–3 μm)	continuous	1 pyranometer, 1 pyrheliometer (0.3–3 μm)	continuous	2 pyranometer (0.3–3.2 μm direct and diffuse)	continuous
			1 pyrgeometer (4–40 μm)	continuous	1 pyrgeometer (4–40 μm)	continuous	1 pyrheliometers (0.3–3.2 μm)	continuous
			shadow-band radiometer (7-λ)	continuous			1 pyrgeometer (4.5–42 μm)	continuous

[a]Total suspended particulate, TSP; particulate matter, P. M.; Isokinetic Particle Collector, IPC [see *Rajot et al.*, 2008].

Figure 4. (left) FAAM BAe146 aircraft. The aerosol and cloud physics probes are visible mounted on the wing pylon as highlighted by the red circle. (right) ULA with the LAUVA lidar in horizontal pointing mode highlighted by the red circle.

period of DABEX and AMMA SOP0 as the prevailing wind speed and direction are important for understanding the transport of both mineral dust and biomass burning aerosol from the source regions across the continent. We concentrate on the January period as this is the most relevant for both DABEX and AMMA SOP0.

[20] Figure 6 shows the wind speed and direction as determined by radiosonde ascents from Niamey, Niger, during January 2006. The near surface (1000–900 hPa) winds are generally from the northerly easterly quadrant throughout January (indicated by the red/orange yellow colors in Figure 6, bottom) and the winds veer with height indicating warm advection from the south at upper levels. There are two exceptions to this; during 17–20 January and to a lesser extent during 29–31 January, the near surface flow reverses and the flow is from the southwesterly quadrant (indicated by the blue colors in Figure 6, bottom). *Rajot et al.* [2008] shows definitive evidence of advection of biomass burning to the Banizoumbou site during the first of these periods by using back-trajectory modeling and analyzing the ratio of the aerosol number to the mass concentrations.

[21] It appears that these periods of low-level southerly flow that draw low-altitude biomass burning aerosol into the Niamey region are associated with a northward shift in the low-level convergence zone from it's more usual position at 10°N to 15°N–20°N. This shift is associated with tropical/extratropical interactions generated by an extratropical

Table 4. Dedicated Aerosol Microphysics, Optical Properties and Chemical Composition Instrumentation, Radiation Instrumentation, and Trace Gas Chemistry Instrumentation Deployed on the BAe146 Aircraft During DABEX/AMM SOP0[a]

	Instrument	Details	Comment
Aerosol microphysics	PMS PCASP	size: 0.05–1 μm radius	wing-mounted
	FFSSP	size: 1.5–20 μm radius	wing-mounted[b]
	Small ice detector (SID-1)	size: 1–30 μm radius	wing-mounted[b]
	SID-2	size: 1–30 μm radius	wing-mounted[b]
	TSI CPC3025	size: > 6 nm radius	cabin
	CVI PCASP	size: 0.05–5 μm radius	cabin: aerosol mode
	CVI CPC3010	size: >20 nm radius	cabin
	CCNC	0.1 to 1% supersaturation	cabin
Optical properties	Radiance Research PSAP	wavelength, λ = 0.568 μm	aerosol absorption
	TSI 3563 Nephelometer	λ = 0.45, 0.55, 0.70 μm	dry aerosol scattering
Chemical composition	Filters	Unit 1: 0.4 and 10 μm Nuclepore Unit 2: 0.4 μm Nuclepore and double quartz	SEM/TEM analysis, wavelength-dependent X-ray fluorescence (WD-XRF) and particle size/shape/aspect ratio
	Quadrupole Aerodyne Aerosol Mass Spectrometer (Q-AMS)	particles 40–700 nm aerodynamic diameter	organic and inorganic volatile and semivolatile aerosols
	VACC	temperature range: 50–700°C PCASP-X (0.05–1.5 μm radius)	volatility and water uptake
Radiation	Eppley radiometers	clear dome: λ = 0.3–3 μm	upwelling and downwelling irradiances
	Shortwave Spectrometer (SWS)	red dome: λ = 0.7–3 μm	pointable. resolution: 3.2 nm to 948.7 nm, 6.3 nm thereafter upwelling resolution: 3.2 nm up to 948.7 nm
	Solar Hemispheric Integrating Measurement System (SHIMS)	spectral radiances at 303.4 nm to 1706.5 nm spectral irradiances at 303.4 nm to 1706.5 nm	
Trace gas chemistry	TECO 49 UV photometric	ozone	
	Aero-Laser AL5002	CO	
	TECO42	NO, NO_2	detection limit <2 ppbv
	TECO 43C	SO_2	

[a]For a more complete description of the instrumentation refer to: http://www.faam.ac.uk/public/instrumentation.html.
[b]Operational difficulties apparent subsequent to analysis.

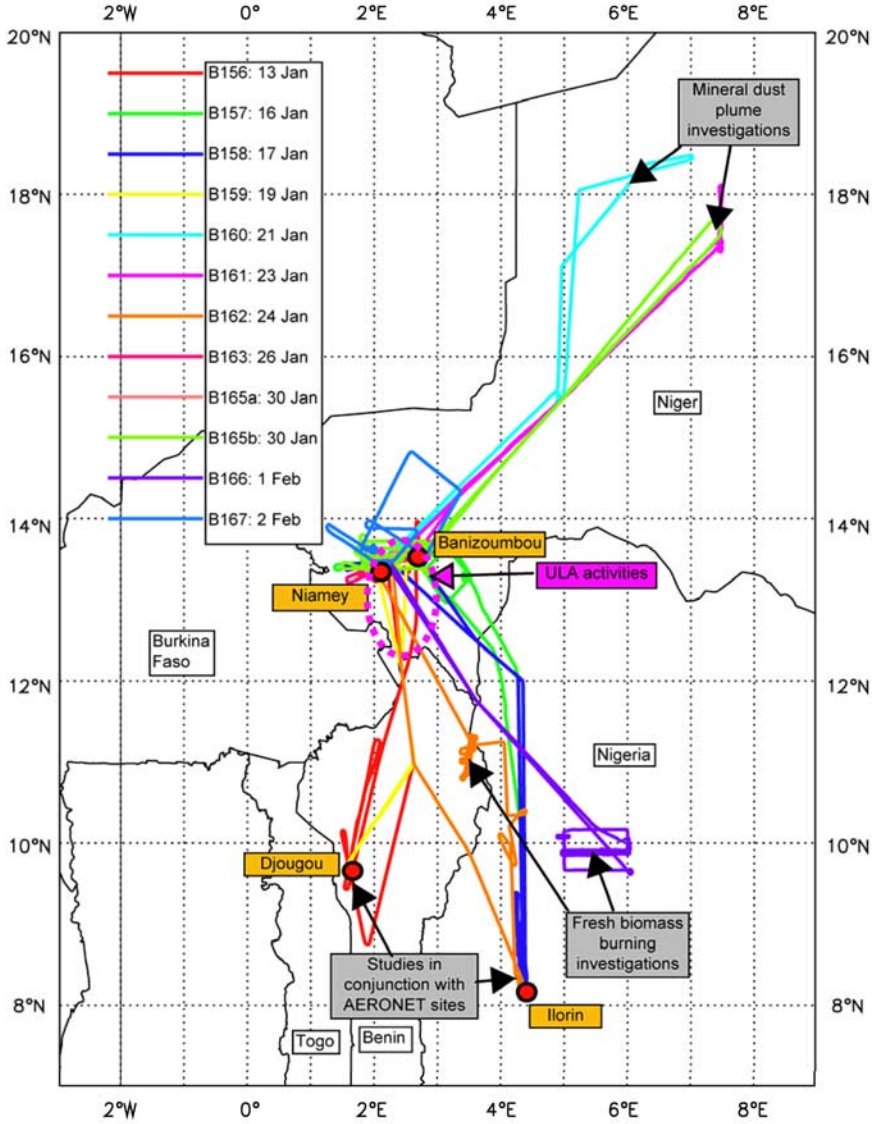

Figure 5. Flight track of the BAe146 during dedicated DABEX/AMMA SOP0 scientific flights. The position of the Ilorin, Banizoumbou, Djougou, and Niamey AMF sites are also marked. The operating area of the ULA is shown by the purple dashed line.

trough to the northwest of the African continent during these two time periods which are characterized by upper level and midlevel clouds in a subtropical jet streak and the development of a tropical plume [*Knippertz*, 2005].

[22] On a more regional scale, Figures 7a and 7b shows the diurnal mean wind speed and direction for January 2006 across West Africa from Met Office global model analyses (generated every 3 h) at 610 m and at 3130 m. The winds at these levels were chosen as they correspond to the approximate peak in the mineral dust loading and biomass burning aerosol loading over the period observed from aircraft and lidar observations [*Johnson et al.*, 2008b; *Pelon et al.*, 2008; *Heese and Wiegner*, 2008]. The mean wind speed and variability at each level will be discussed in turn.

[23] The diurnally averaged wind data show easterly or northeasterly 610 m mean flow over much of Chad and Niger and northeast Nigeria. The effect of orography is demonstrated by the channeling of the 610 m winds to the south of the mountainous Hoggar and Tibesti plateaux. Over Niamey, the 610 m mean wind direction has a strong easterly component indicating that Niamey is downwind of some significant mineral dust source regions such as the Bodélé depression in western Chad [e.g., *Washington et al.*, 2006; *Todd et al.*, 2007]. *Parker et al.* [2005] show a strong influence of diurnal cycle in the surface and 600 m winds over Niger. Our analyses for January 2006 suggest that the general 610 m wind direction remains similar throughout the diurnal cycle, but that the wind speed increases by a factor of approximately 2 between 1800 UTC and 0600 UTC over much of Niger, Burkina Fassau, and Chad, showing qualitative agreement with the findings of *Parker et al.* [2005].

[24] While the mean wind speed and direction is useful for determining the mean flow, it does not provide information on the variability of the wind speed and direction; wind roses are therefore also provided. At 610 m the least

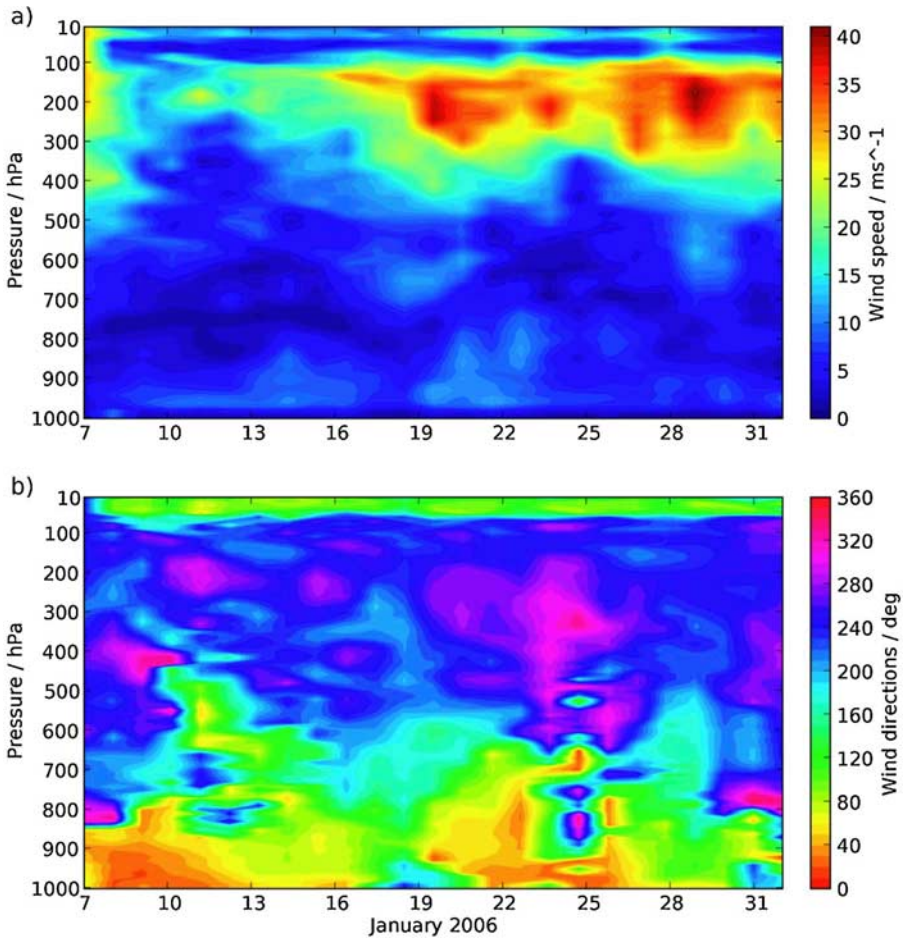

Figure 6. Wind (a) speed and (b) direction determined from 6-hourly radiosonde ascents from Niamey.

variability in the wind speed and direction occurs around the latitude of Niamey (Figure 7c, middle row) where the winds are predominantly easterly or northeasterly; these areas also typically experience 610m winds of greater than 5 m s^{-1}. To the north of Niamey (Figure 7c, top row) the winds are more variable in direction though still typically in excess of 5 m s^{-1}. To the south of Niamey (Figure 7c, bottom row), the wind speed is typically lighter and more variable, with a significant southerly component. Once more this analysis suggests that Niamey will seldom be influenced by biomass burning aerosol at the surface [*Rajot et al.*, 2008].

[25] Figure 7b shows that, at an altitude of 3130 m, the latitudes around 12°N–17°N are at the interface between strong westerly winds to the north and strong easterly winds to the south. The diurnal variation in both the strength and direction of the wind at 3130 m in the model analyses is insignificant.

[26] At 3130 m (Figure 7d) the wind roses clearly show the shift from predominantly strong westerly winds to the north of Niamey to strong easterlies south of Niamey. At the latitude of Niamey (Figure 7d, middle row), there is a small, but significant southerly mean wind component which indicates that aerosol at this level would generally be transported northward by the prevailing meteorology. Thus biomass burning aerosol which originates at latitudes south of 11°N (Figure 1), may be advected hundreds of kilometers north of its origin. This is the reason why biomass burning aerosol that is detected in the regions of active fires such as the Djougou site [e.g., *Mallet et al.*, 2008; *Pelon et al.*, 2008] and Ilorin site [*Nwofor et al.*, 2007] is so frequently detected at altitude over Niamey [e.g., *Heese and Wiegner*, 2008; *Johnson et al.*, 2008b] site.

[27] Figure 8 shows two examples of vertical profiles of aerosol scattering (β_{sca}). Figure 8a is from a vertical profile close to Niamey, while Figure 8b shows a vertical profile at around 18°N, 7°E. While the relative contribution of biomass burning and mineral dust to the aerosol optical depth varies considerably between the two profiles, both profiles show mineral dust aerosol in the lowest 1–1.5 km with overlying biomass burning aerosol clearly evident at higher altitudes as evidenced by the difference in the wavelength dependence of the scattering. The wavelength dependence of the scattering is defined by the Angstrom exponent, Å,

$$\mathring{A} = -\ln(\tau_1/\tau_2)/\ln(\lambda_1/\lambda_2), \quad (1)$$

where τ is the AOD at wavelength λ. Small aerosol particles such as biomass burning aerosols interact more strongly with the shorter wavelengths of solar radiation while mineral dust particles interact with all solar wavelengths approximately equally. Consequently Å for biomass burning is in the range 1 to 1.5 while Å for mineral dust is typically close to zero [e.g., *Johnson et al.*, 2008a; *Pelon et al.*, 2008].

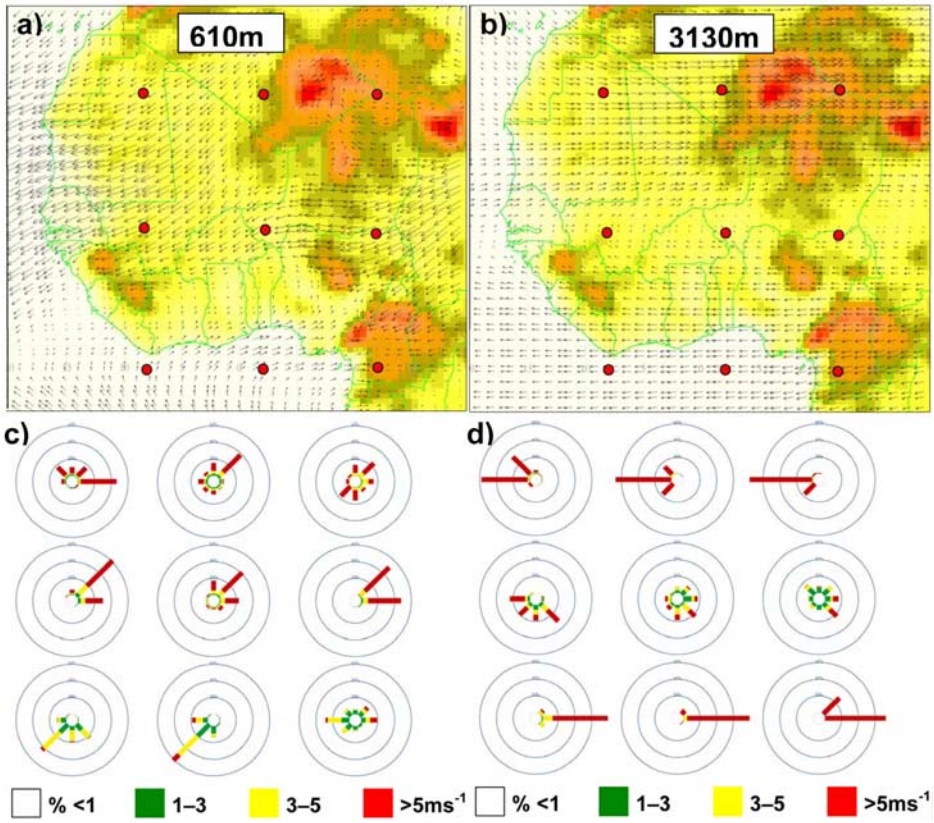

Figure 7. Wind fields from UK Met Office analysis for January 2006. (a, b) Mean flow superimposed upon the model orography, and (c, d) wind roses for the nine positions marked which are centered at Niamey ±10° latitude and Niamey ±10° longitude. Brown, orange, and red correspond to elevations exceeding 450, 900, and 1500 m, respectively. The model levels corresponds to approximately 610 m (Figures 7a and 7c) and 3130 m AGL (Figures 7b and 7d) which approximately corresponds to the peak of the mineral dust loading and biomass burning loading observed by *Johnson et al.* [2008b]. The bold circles on Figures 7c and 7d correspond to 20% probability for the inner circle, 40% for the middle circle, and 60% for the outer circle and are cumulative.

[28] *Pelon et al.* [2008] show that the maximum biomass burning aerosol optical depth is frequently over the ocean regions in the Gulf of Guinea which may be due to different intensities of burning and advection of biomass burning aerosol from source regions to the east in the east and northeasterly flow. The flow patterns in Figure 7 also explain why biomass burning aerosol is also an important contributor to the aerosol optical depth during January and February 2006 at the M'Bour site in Dakar with elevated biomass burning aerosol layers extending from 1 to 4 km being readily detected in the lidar and by analysis of the Angstrom exponent derived from AERONET [*Derimian et al.*, 2008]. The 3130 m mean wind direction shown in Figure 7b shows that the biomass burning aerosol may be advected out over the Atlantic ocean before returning to the M'Bour site in weak southwesterly flow. The very low aerosol optical depths over Tamanrasset during February 2006 (aerosol lidar not operational during January 2006), suggests that the biomass burning layers do not penetrate as far north as Tamanrasset in southern Algeria [*Cuesta et al.*, 2008] although it may be transported at similar latitudes over eastern Niger and Chad by the perturbed synoptic flow.

[29] The relative stability/instability of the atmosphere completes the picture of biomass burning and mineral dust transport. Mean January 2006 tephigrams from Met Office global analyses for 12UTC are plotted for Parakou (9.33°N, 2.63°E), Niamey (13.5°N, 2.1°E), and Kidal (18.3°N, 1.2°E) in Figure 9 (for geographic locations see Figure 3). The Parakou ascent shows considerably more moisture close to the surface (around 16 g/kg) than at Niamey (around 5 g/kg), and the extremely dry conditions at Kidal (3 g/kg). The lowest levels of the Parakou ascent follow the dry adiabat to around 900 hPa and there is a relatively low lifting condensation level (LCL), at around 845 hPa. The Normands construction on the Parakou tephigram [*Normand*, 1938] indicates high convective available potential energy (CAPE), and convective instability extending to the tropopause, associated with the deep convection of the ITCZ to the south of the region. For the Parakou profile, deep convection can be initiated by surface temperatures in excess of approximately 35°C; values that are frequently exceeded. This suggests that the effect of plume buoyancy from the fires themselves has relatively little effect on the lifting of the biomass burning aerosols; it is the inherent instability of the atmosphere

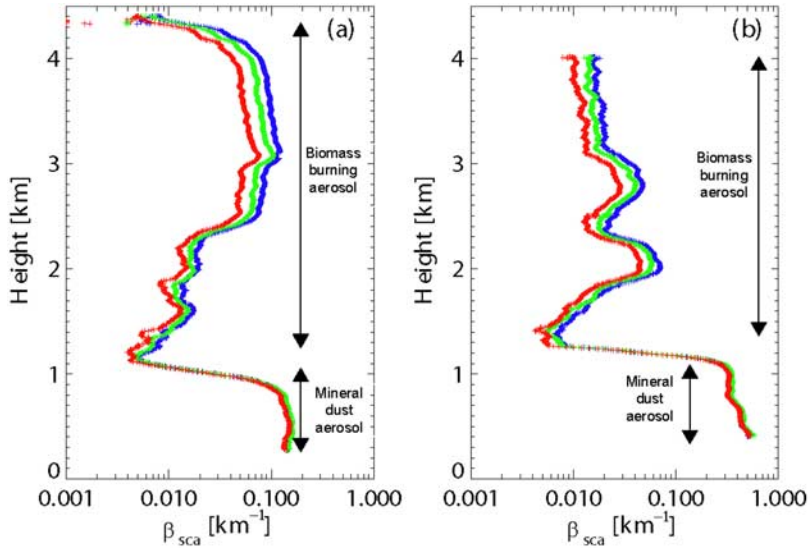

Figure 8. Profiles showing the red (650 nm), green (550 nm), and blue (450 nm) scattering (β_{sca}) from the biomass burning layer and mineral dust layer from (a) profile 17 close to Niamey and (b) profile 10 at around 18°N, 7°E on flight B161 of the BAe146 aircraft. The biomass burning layer is distinct from the mineral dust layer as characterized by the larger Angstrom exponent (larger wavelength dependence [see also *Osborne et al.*, 2008; *Johnson et al.*, 2008a].

that appears to be more important. At Niamey the lowest part of the ascent, to around 900 hPa, follows the dry adiabat, followed by a transition to a profile following the moist adiabat at pressures less than 650 hPa. Very high boundary layer temperatures in excess of 45°C would be needed in order to mix the Niamey profile to a pressure of around 650 hPa. The biomass burning layers were found in the intermediate layers between 900 hPa and 600 hPa. The low humidity of the mean Niamey profile, and the high LCL are consistent with the observed absence of shallow or deep moist convection, and therefore a lack of vertical mixing between the aerosol layers above the dry convective boundary layer. At Kidal, the remains of the nocturnal inversion are seen in the profile ascent which is cool, as well as being very dry and stable at lower levels. The strong static stability would prevent dust from mixing vertically into the free troposphere, keeping it in a layer from the surface to 900–850 hPa.

[30] Of course there will be many day-to-day variations in the position of the mineral dust and the overlying biomass burning as evidenced by the variability in the wind fields shown in Figures 7c and 7d. This can be demonstrated by the two CALIPSO lidar backscattering cross sections shown for 7 and 18 January 2007 (CALIPSO was not operating during DABEX). These profiles were selected because of their proximity to Niamey, the lack of cloud in the area of interest, and the presence of a relatively dusty near-surface layer. Both of these cross sections show lower dust layers capped at approximately 1 km altitude south of approximately 20°N and upper layers of biomass burning influenced aerosol aloft at altitudes of approximately 4–5 km (Figure 10). The depolarization ratio (not shown) of the mineral dust (0.3–0.5) differs considerably to that from of biomass burning (0 to 0.1) influenced aerosol in the CALIPSO data, enabling separation between the large particle dominated dust and the small particle dominated biomass burning aerosol.

[31] Nephelometer data from a transect Niamey-Djougou on the BAe146 during flight B159 at an altitude of around 500 feet AGL [*Pelon et al.*, 2008] confirms the general situation. This transect clearly shows the position of the "dust front" at 10°N which marks the transition from mineral dust dominated to biomass burning dominated air masses. *Pelon et al.* [2008] also analyze lidar and satellite data to show that biomass burning aerosols have significant concentrations over the ocean in the Gulf of Guinea, which suggests that upper level circulation plays a significant role in the transport of aerosols southward toward the Inter-Tropical Convergence Zone (ITCZ).

[32] The LAUVA backscatter lidar stationed at Niamey airport [*Chazette et al.*, 2007] allows observation of the dust transport at far higher spatial and temporal resolution than the CALIPSO measurements. Figure 11 shows the progression of a dust front through the Niamey region on 23–24 January 2006.

[33] The first evidence of the dust front occurs between 2030 and 2100 UTC on 23 January (around 23.87 on the time axis of Figure 11): at this time there is evidence of dust being lifted to around 250 m above ground level (a.g.l.) in the space of a few minutes, possibly at the head of a shallow density current or convergence line, and then ascending to around 550 m a.g.l. over the next 2 h. Following this event, there is a general increase in low-level dust loadings, and evidence of lifting: a major event occurs between around 0130 and 0330 UTC at Niamey, when dust is lifted to an altitude of around 500 m a.g.l. The typical slope of the dust features in Figure 11 represent ascent rates of around 10–30 cm s^{-1}: although this is slower than the ascent rates associated with the head of a density current, it remains a very high rate of ascent

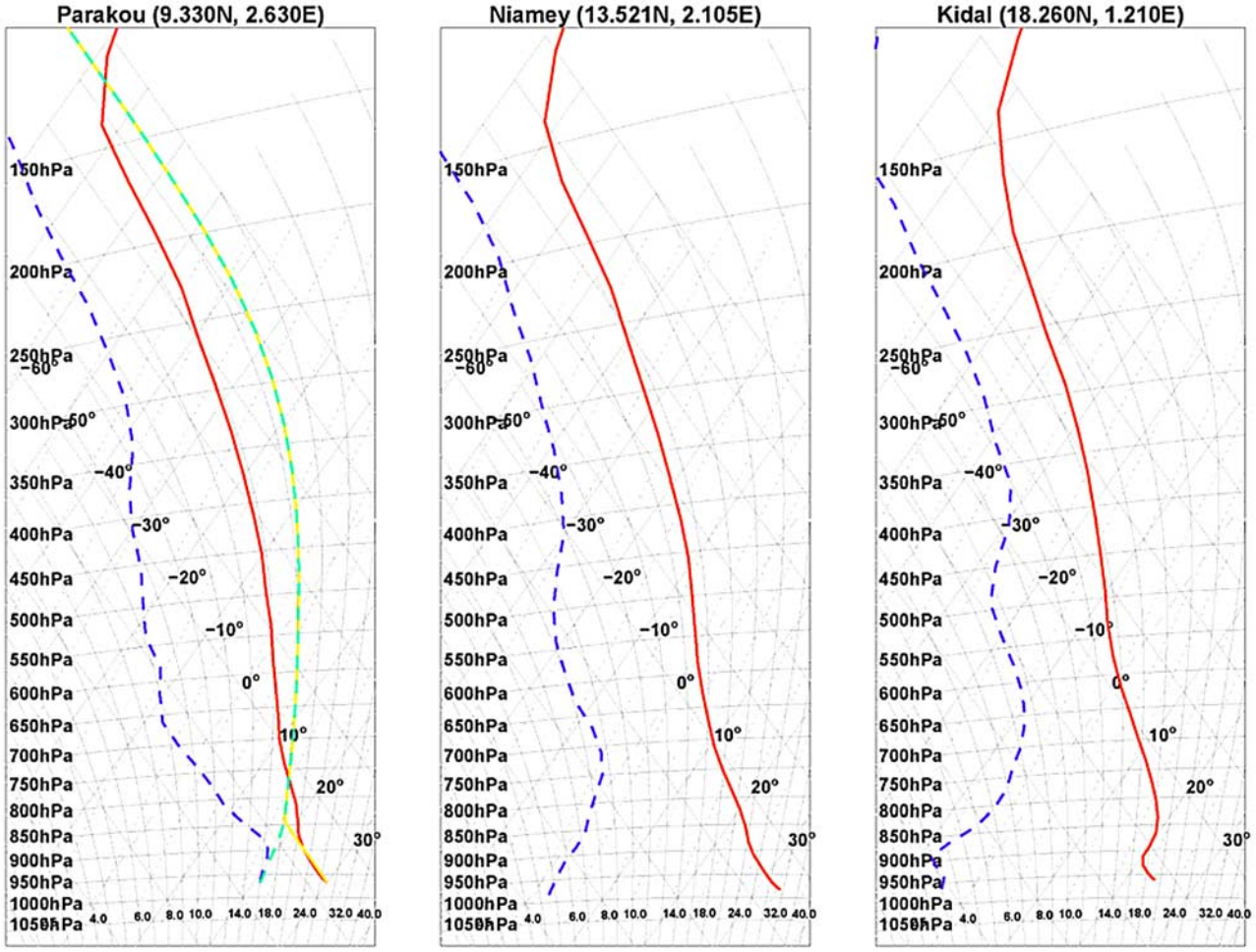

Figure 9. Tephigrams of the mean temperature (red solid line) and dew point (blue dashed line) profiles at 1200 UTC for January 2006, extracted from the Met Office global model forecasts at T + 0. The Normand's point construction is shown on the Parakou ascent (shown by the green/yellow lines).

for the tropics and demonstrates significant convergence throughout the period.

[34] AMF thermodynamic profiles (not shown) suggest that the strongest air mass change in the lowest 500 m occurs between 2000 and 2100 UTC, when 200 m dewpoint falls by some 2°C and 200 m temperature falls by around 0.5°C. This air mass change coincides with the first, rapid dust-uplift event observed in the lidar data and provides further support for a weak density current or convergence line having crossed Niamey. We infer that warmer air is being forced to rise above undercutting colder, drier air.

[35] The convergence leading to the ascent of dust seen in Figure 11 is not associated with cold pools from the moist convective structures which are thought to contribute significantly to dust production during the monsoon season [e.g., *Flamant et al.*, 2007; *Marsham et al.*, 2008]. The origin of these convergent flows requires further investigation, but they may be a product of larger-scale regional dynamics (as demonstrated in the laboratory by *Linden and Simpson* [1986]) and they could be influenced by the diurnal cycle of heating over the topography of the region.

[36] Putting together the flow and stability data enables a simplified meridional-vertical cross section of the meteorological conditions affecting aerosol transport to be developed (Figure 12).

[37] Mineral dust is transported from the Sahara desert in low-level east-northeasterly flow and funneled around the Tibesti and Hoggar plateaux. The biomass burning particles emitted by anthropogenic activities south of 11°N are emitted in a region of convective instability which is subject to weak southerly advection. As this biomass burning air moves north it overrides the cooler, drier mineral dust laden air (as in Figure 7b). Note that observations by the BAe146 of the altitude of the top of the biomass burning influenced layer are around 2.5 km over in the source region in western Nigeria and Benin [e.g., *Pelon et al.*, 2008; *Mallet et al.*, 2008], but at approximately 3.5 km by the latitude of Niamey [*Johnson et al.*, 2008b], and in excess of 4 km at 18°N (Figure 8). Thus the biomass burning layer tends to be lifted to higher altitudes as it moves farther north. Note that the boundary between the warm air laden with biomass burning products and the cooler Saharan air laden with dust (solid line in Figure 10) is a different boundary to the Intertropical front (ITF). We chose to call this boundary the "Harmattan front." *Hastenrath and Lamb* [1977] show a similar schematic diagram during the monsoon flow during

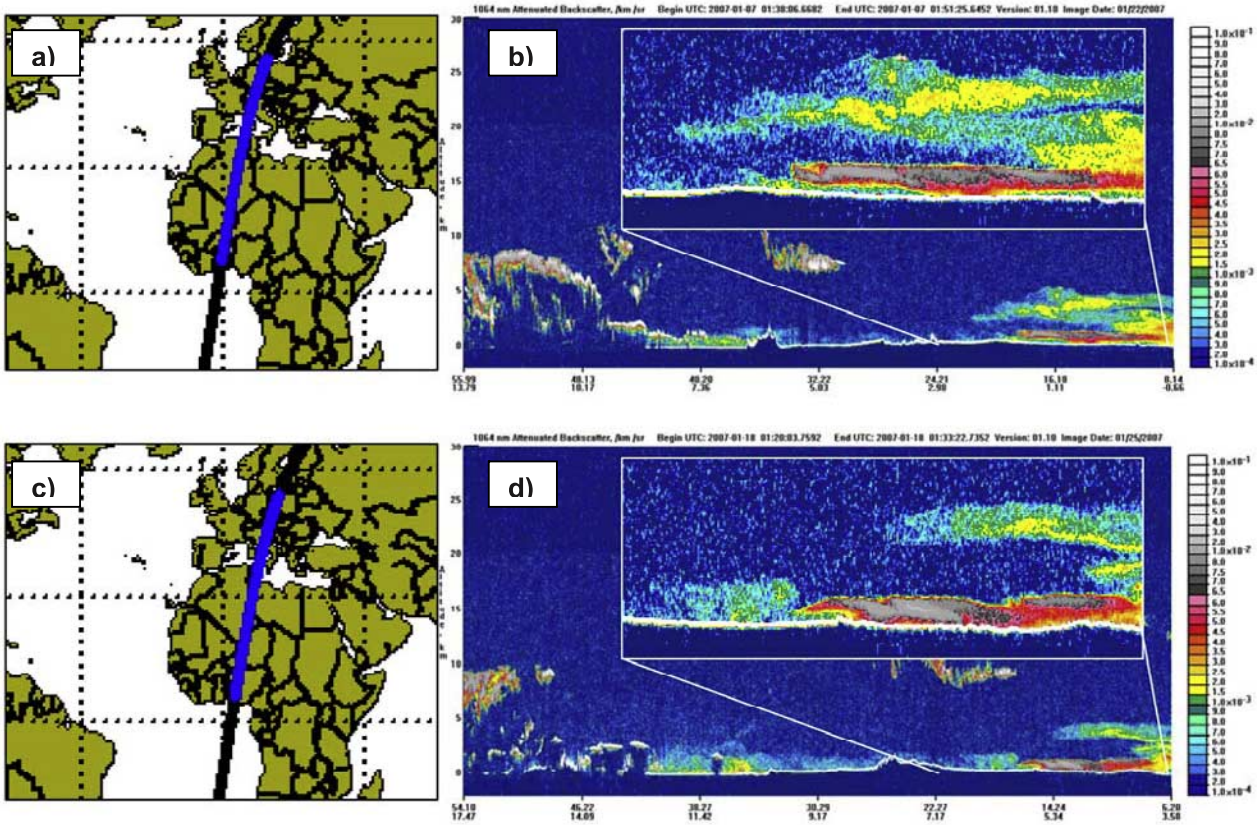

Figure 10. Aerosol backscatter from the CALIPSO lidar (1032 nm) during transects across N Africa: (a, b) 7 January 2007 and (c, d) 18 January 2007. The highlighted boxes in Figures 10b and 10d show close-ups of the area from approximately 22°N to 5°N. The dust layers are shown by red and grey (backscatter > 4–10 × 10^{-2}km^{-1}sr^{-1}), while yellow represents biomass burning influenced aerosol (backscatter > 1–2 × 10^{-2}km^{-1}sr^{-1}).

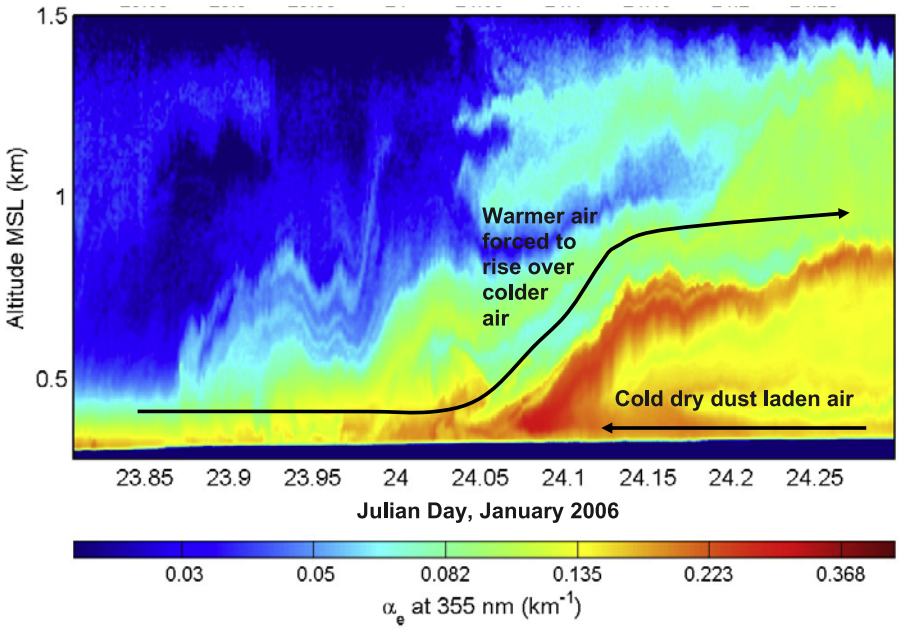

Figure 11. LAUVA backscatter lidar image showing the progression of a dust front through Niamey during 23–24 January. The lidar was sited at Niamey airport; α_e is the aerosol extinction in per kilometer.

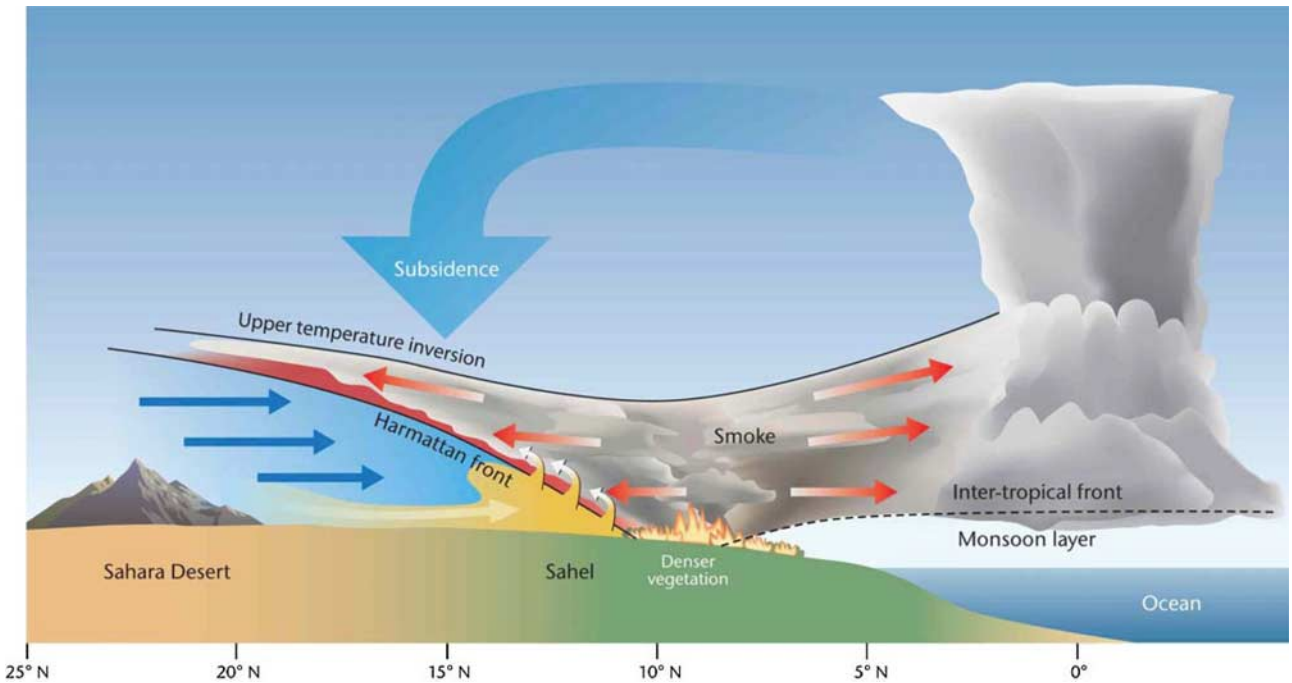

Figure 12. Schematic zonal cross section showing the northward transport of biomass burning aerosol in warm, ascending air (red arrows) and the westward/southward transport of mineral dust in a cooler airflow channeled by the mountainous regions to the north (blue arrows). The "Harmattan front" is shown by the solid line which marks the boundary between the two air masses with arrows representing mixing of the dust with the biomass burning smoke. The intertropical front marks the boundary between the moist monsoon air and the smoke-laden air. A deep convective cloud associated with the ITCZ is represented to the south.

July–August in the west African region, but the position of the ITCZ is displaced farther to the north. *Slingo et al.* [2008] suggest that the position of the ITF in July–August 2006 is approximately 16°N–20°N across much of west Africa, while in January, Figure 10 shows that the ITF lies some 10° farther south at around 9°N, and slopes upward toward the south.

5. Overview of Aerosol Chemical, Physical, and Optical Properties, and the Associated Radiative Effects

[38] Aerosol chemical, physical and optical properties were investigated from a number of surface and airborne platforms during DABEX and AMMA SOP0. The chemical analysis of both mineral dust and biomass burning aerosols from the BAe146 relies on scanning and transmission electron microscopy (SEM and TEM) and wavelength dispersive X-ray fluorescence (WD-XRF) analyses of single particles on filter samples [*Chou et al.*, 2008; *Formenti et al.*, 2008], while the Aerodyne AMS enables determination of the changes in chemical composition of biomass burning aerosols as they age [*Capes et al.*, 2008].

[39] Chemical analysis is also presented from filters collected at the Banizoumbou site using WD-XRF [*Rajot et al.*, 2008; *Formenti et al.*, 2008]. *Chou et al.* [2008] determine that the chemical composition of mineral dust particles was dominated (80% by number) by aluminosilicates in the form of illite, kaolinite and quartz, and that 4% of the submicron particles contained iron oxides. The electron microscope analysis allows determination of the average aspect ratio (the ratio of the geometric length to the geometric width) of mineral dust particles, finding a median value of 1.7 with implications for modeling the optical properties via a collection of prolate and oblate spheroids as recommended by *Mishchenko et al.* [1997], and performed by *Osborne et al.* [2008]. This aspect ratio supports the approach in AERONET inversion products (level 2) which uses a mix of prolate and oblate spheroids to model aerosol optical properties [*Dubovik et al.*, 2006]. A number of airborne diatoms are also detected on the filters suggesting a contribution to mineral dust loading from the Bodélé depression; these diatoms were a major component of dust measured by *Todd et al.* [2007]. *Formenti et al.* [2008] make comparisons of the chemical composition of mineral dust measured during DABEX on the BAe146 with measurements performed during the DODO [*McConnell et al.*, 2008] campaigns based in Dakar, Senegal. They find consistency between the BAe146 DABEX samples and the Banizoumbou surface super site measurements during DABEX, but significant differences in chemical composition with potassium rich illite clays contributing in measurements over Senegal and Mauritania.

[40] *Capes et al.* [2008] analyze the chemical composition of biomass burning particles from Q-AMS measurements on board the BAe146 showing some significant changes in the detected mass spectra over time: analysis

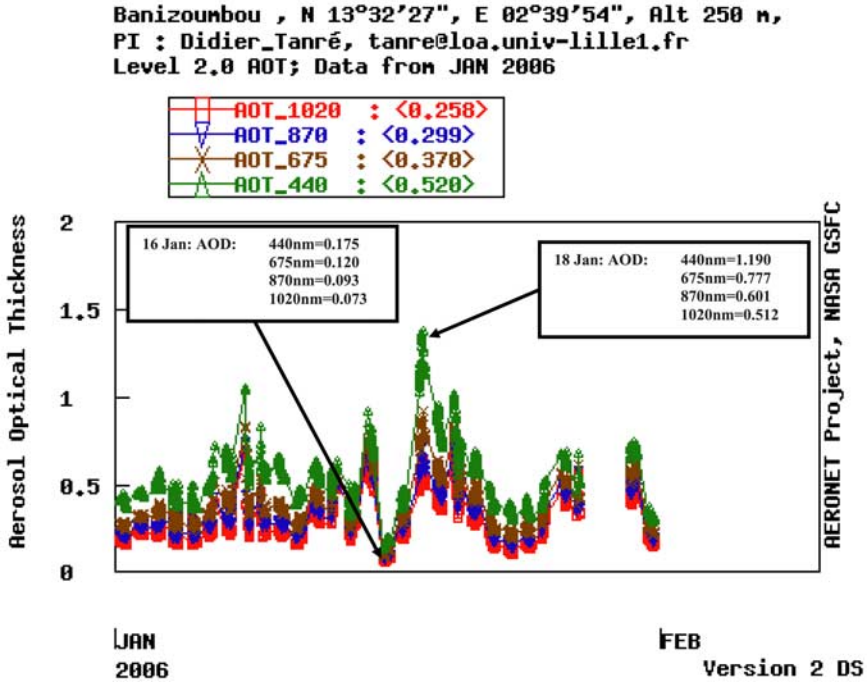

Figure 13. Aerosol optical depth at 440, 675, 870, and 1020 nm diagnosed from the Banizoumbou surface site for January 2006. The lowest aerosol optical depths (AODs) occur on 16 January, while the highest AODs occur on 18 January.

of the changing relative contributions to the total mass from constituents such as levoglucosan, saturated hydrocarbons, aldehydes and ketones is presented. The biomass burning aerosol particle size distribution shifts to larger size as the particles age, but the ratio of organic carbon (OC) to excess carbon monoxide (ΔCO) appears to be constant which is in sharp contrast to results for industrial regions [*Crosier et al.*, 2007]. *Capes et al.* [2008] postulate that chemical transformation of the organic carbon and condensation/evaporation of the aerosol may all be important in maintaining the OC/ΔCO ratio.

[41] The optical properties of both mineral dust and biomass burning received considerable attention during DABEX and AMMA SOP0. *Johnson et al.* [2008a] and *Osborne et al.* [this issue] investigate the optical properties of biomass burning aerosols and mineral dust respectively from instruments on the BAe146. *Johnson et al.* [2008a] find that biomass burning aerosol is significantly more absorbing than that measured using the same instruments during SAFARI-2000 [*Haywood et al.*, 2003a], while *Osborne et al.* [2008] reiterates that submicron mineral dust is only very weakly absorbing; similar results have been recently found for both Saharan dust and Asian dust [*Haywood et al.*, 2003b; *Tanré et al.*, 2003; *McConnell et al.*, 2008, *Clarke et al.*, 2004; *Huebert et al.*, 2003]. The study of *McConnell et al.* [2008] shows the importance of including the coarse mode mineral dust particles in strong dust plumes; the results for DODO during August 2006 show a significant decrease in single scattering albedo from 0.98 to 0.90 at 0.55 μm upon inclusion of the coarse mode. *Johnson et al.* [2008a] show that there appears to be little variation in the aerosol single scattering albedo with age, which suggests that the chemical transformation of the organic carbon and condensation/evaporation of the aerosol do not significantly effect the absorption properties of the biomass burning aerosols. This is contrary to the findings of *Abel et al.* [2003] who showed that the single scattering albedo of biomass burning aerosol from a discrete plume became less absorbing with age presumably owing to the condensation of volatile gases onto the primary biomass burning aerosol particles. AERONET inversions (version 2 [*Dubovik et al.*, 2002]) of the single scattering albedo from Banizoumbou, Djougou and Ilorin for multiple Januarys show that there is no significant difference in the solar absorption between the sites with single scattering albedos of 0.85, 0.88, and 0.90 at wavelengths of 440 nm, 670 nm, and 870 nm, respectively. However, at the well established site of Mongu, Zambia (10 years of data) where biomass burning is prevalent during July–September (Figure 1), the August mean single scattering albedo is 0.85, 0.81, and 0.78 at the same wavelengths. Thus the wavelength dependence of the single scattering albedo is reversed between areas of northern Africa and southern Africa. As explained by the modeling work of *Myhre et al.*, 2008), this may be explained by the ubiquitous presence of mineral dust in the column of atmosphere at the northern Africa sites which causes the single scattering albedo to more closely resemble that of mineral dust at longer wavelengths.

[42] Surface-based observations of biomass burning aerosol, mineral dust aerosol and columnar integrations via remote sensing retrievals are performed for Djougou [*Mallet et al.*, 2008; *Pelon et al.*, 2008], M'Bour [*Derimian et al.*, 2008], and Tamanrasset [*Cuesta et al.*, 2008]. *Mallet et al.* [2008], and *Derimian et al.* [2008] also present results from modeling atmospheric radiative transfer to show the con-

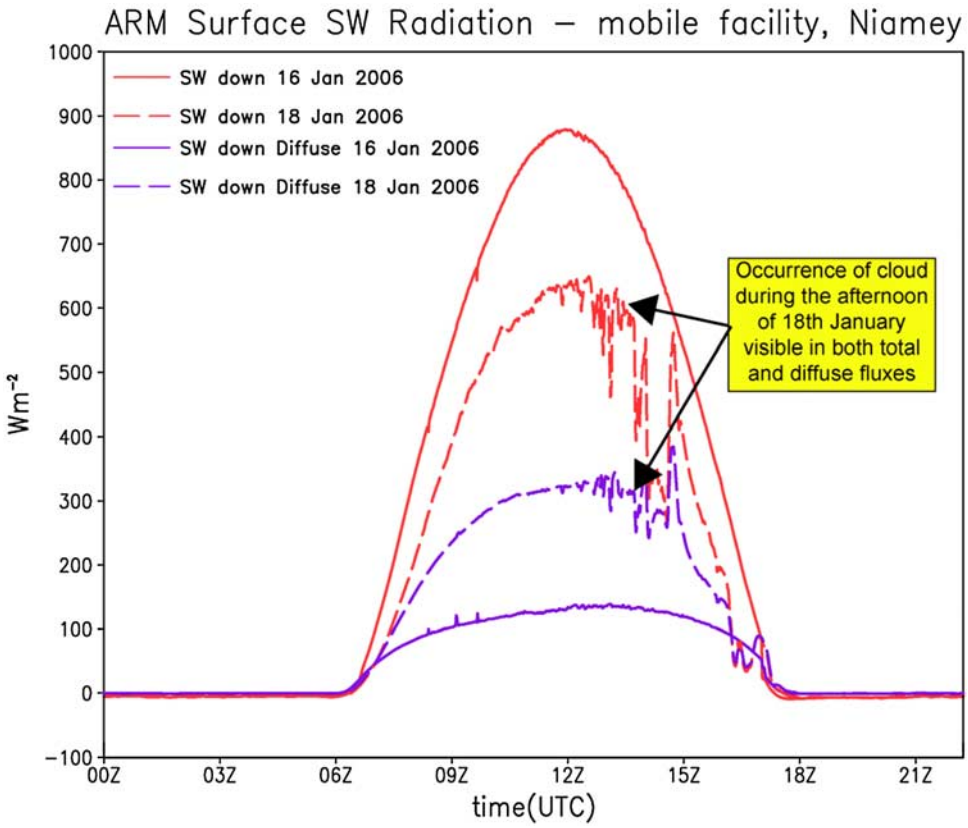

Figure 14. Total (red) and diffuse (purple) irradiances at the surface as determined from measurements made with solar pyranometers at the AMF located in Niamey, Niger, for 16 (solid line) and 18 (dashed line) January 2006. The top of atmosphere flux at local noon varies by less than 0.5 W m^{-2} between the 2 days.

sistency of the modeled and calculated radiative fluxes and providing radiative closure. The importance of considering both biomass burning aerosols and mineral dust is further evidenced by *Milton et al.* [2008] who show that, at Niamey during DABEX/AMMA SOP0, approximately 50% of the reduction of surface solar insolation is due to biomass burning aerosols and 50% is due to mineral dust aerosols, with the contribution from mineral dust increasing as the biomass burning activity decreases in February/March. A similar decrease in the biomass burning contribution is seen from the analysis of Angstrom exponents from the AERONET site at Djougou as the biomass burning intensity decays in February [*Pelon et al.*, 2008].

[43] The influence of aerosols upon surface radiation can be inferred without performing radiative transfer calculations by comparing the solar irradiance at the surface for a low-AOD day against that of a turbid, high-AOD day. Figure 13 shows continuous measurements of the aerosol optical depth throughout January as measured from the Banizoumbou AERONET site. On the 16 January the AOD at 440 nm was 0.17 while on 18 January the corresponding AOD was 1.19.

[44] The solar irradiance data from the nearby Niamey AMF for the two days (total and direct) is shown in Figure 14. During the second half of 18 January, cloud moved in and data from 12UTC should be ignored as it fails to isolate aerosol direct effects only owing to cloud contamination. The total flux decreases by 230 W m^{-2} or a factor of 1.36 from 879 W m^{-2} to 648 W m^{-2} with more diffuse irradiance as evidenced by the increase from 139 W m^{-2} to 330 W m^{-2} at around 1200 UTC. A simple $\Delta SW/\Delta AOD$ calculation assuming a linear dependence between the reduction in solar irradiance and the aerosol optical depth reveals that the normalized instantaneous midday surface forcing is approximately 225 W m^{-2} per unit aerosol optical depth. Assuming that the aerosol composition during 16 and 18 January is representative of the site (the Angstrom exponent between 440 and 1020 nm is 1.0 for 18 January and 0.83 for the whole month of January), the effect on the surface irradiance for January at 1200 UTC can be approximated as a reduction of 117 W m^{-2}. Of course, this is a very simple and limited analysis; *Mallet et al.* [2008], *Derimian et al.* [2008], and *Milton et al.* [2008] provide far more detailed assessments of the effect of aerosols upon the surface radiation budget.

6. Overview of Modeling and Satellite Observation Activities

[45] *Myhre et al.* [2008] provide an assessment of global modeling study for emissions of mineral dust, black carbon and primary and secondary organic aerosols from biomass burning. The study uses a 1 × 1 degree horizontal resolution version of the Oslo Chemical Transport Model

(CTM), and concludes that the mean model fields show reasonable agreement with the mean observations during the January–February 2006 period. Besides the geographic distribution of the aerosol, key optical features such as the wavelength dependence of the biomass burning/mineral dust combination are well represented. The vertical profile of the biomass burning and dust layers presented by *Myhre et al.* [2008] does show that the biomass burning aerosol layer contributes a more significant optical depth at higher altitudes, but also shows that the model tends to transport mineral dust at too high an altitude when compared to observations from aircraft measurements and from lidars [*Johnson et al.*, 2008b; *Heese and Wiegner*, 2008]. The Met Office climate model HADGEM2 [*Bellouin et al.*, 2007] is also used to simulate biomass burning aerosol and mineral dust during the DABEX period and it represents the vertical profile of the dust and biomass burning aerosol well, although the strength of the biomass burning plume is very dependent upon the emission source data set [*Johnson et al.*, 2008b]. *Johnson et al.* [2008a, 2008b] show that although biomass burning aerosol may dominate the number concentration to the south of the region, and in elevated plumes transported northward (section 4), there is frequently considerable mixing of biomass burning and mineral dust in external mixtures [see also *Formenti et al.*, 2008]. This is because the biomass burning is frequently injected into an already turbid, dusty environment. Both the Oslo CTM and HADGEM2 appear to represent the external mixing and relative vertical positions of the mineral dust and biomass burning aerosols adequately. A model assessment of the effect of the layering structure upon the radiative forcing of biomass burning aerosols performed by *Johnson et al.* [2008b] indicates that the presence of natural mineral dust enhances the absorption of solar radiation by anthropogenic biomass burning aerosols over the west African region by approximately 10%. The maximum effect is over low-albedo surfaces such as ocean, indicating that the importance of modeling natural aerosols correctly in diagnosing the radiative effects of anthropogenic aerosol [*Bellouin et al.*, 2008].

[46] While DABEX and AMMA SOP0 concentrated their efforts on the period January–February 2006, some of the modeling studies presented in this Special Section center on modeling mineral dust storm events throughout 2006. *Milton et al.* [2008] and *Tulet et al.* [2008] model and the initiation, production, and transport of an intense dust event during March 2006 [see also *Slingo et al.*, 2006]. Both studies use AERONET Sun photometers to assess the performance of the models and highlight the strengths and weaknesses of the modeling efforts. The high temporal resolution dust products from the Spinning Enhanced Visible and Infrared Imager (SEVIRI) provide qualitative estimates of the aerosol optical depth, though these are strongly dependent upon the surface temperature, emissivity and assumed vertical profile of the mineral dust [*Brindley*, 2007]. *Christopher et al.* [2008] uses correlations between the aerosol optical depth from the MultiImaging Spectroradiometer (MISR) satellite instrument and the semiquantitative aerosol index from the Ozone Monitoring Instrument (OMI) satellite instruments to provide additional data for validating aerosol transport models. *Greed et al.* [2008] initially tune the model dust parameterizations within the UK Met Office Mesoscale model to provide a reasonable dust aerosol optical depth for the intense dust event of 7–13 March 2006 [*Milton et al.*, 2008; *Tulet et al.*, 2008]. They then investigate an independent dust event during September 2006 using a combination of the derived OMI/MISR satellite product from *Christopher et al.* [2008], aircraft observations and AERONET, finding that the model portrays skill in forecasting the dust storm position, intensity, and vertical profile for T + 42 h forecasts. Unfortunately, the CALIPSO satellite mission experienced significant delays and was not operational during the DABEX/AMMA SOP0 timeframe. However, *Cuesta et al.* [2008] provide data from the backscatter aerosol lidar which was based at Tamanrasset throughout together with CALIOP to study the dynamics of the Saharan atmospheric boundary layer. Their analysis shows the very different seasonal evolution of the Saharan boundary layer, with dust being confined to a shallow layer (~500 m) during winter and a much deeper boundary layer during summer (up to 6 km), results that are consistent with the findings from the in situ vertical profile measurements during DABEX [*Johnson et al.*, 2008b; *Heese and Wiegner*, 2008] and other measurement campaigns during summer such as SHADE [*Haywood et al.*, 2003b], and DODO [*McConnell et al.*, 2008].

7. Conclusions

[47] This paper provides an overview of the meteorological conditions during DABEX and AMMA SOP0 and a synthesis of the various surface and aircraft based measurements. Analysis of observations and models show that mineral dust was transported into the Sahel from sources in the Sahara desert by the mean east to northeasterly flow at low altitudes. This cool stable air mixes with and undercuts the warmer smoke laden air to the south of the region, forcing the biomass burning aerosol to rise above the dust laden air. The biomass burning laden air is gently advected to the north and is readily detectable several hundreds of kilometers north of the areas of active fires as well as to the south of the fires over the Gulf of Guinea. The atmospheric instability in the biomass burning dominated region appears the predominant factor in lifting the biomass burning layer rather than the additional plume buoyancy from the fires. This conceptual model is based on vertical profiles of aerosol scattering and extinction from aircraft [*Johnson et al.*, 2008b] and lidar [*Heese and Wiegner*, 2008; *Derimian et al.*, 2008], plus radiosonde data and analysis of wind fields from the Met Office Mesoscale model. An example of nephelometer data from the BAe146 showed biomass burning aerosol well to the north of Niamey (Figure 8), whereas observations with a lidar showed dusty air being advected into the Niamey region from the northeast (Figure 11).

[48] Biomass burning aerosol was found to be more absorbing than that measured with the same instrumentation during SAFARI-2000 with a mean single scattering albedo of 0.81 (stdev 0.08) at 0.55 μm while mineral dust aerosol was found to be almost nonabsorbing at solar wavelengths with a mean single scattering albedo of 0.99 ± 0.01 at 0.55 μm [*Osborne et al.*, 2008]. A surprising

result was that the ratio of excess carbon monoxide to organic matter did not vary much during DABEX [*Capes et al.*, 2008]. Further studies into the invariance in the ratio of excess carbon monoxide to organic matter and the invariance of the single scattering albedo of biomass burning aerosol is planned. At the surface site of Djougou a large degree of variability was observed in the single scattering albedo determined from aethalometer and nephelometer measurements. Values ranged from 0.81 to 0.98 (at 0.52 μm) due to the variability in the relative contributions of biomass burning and mineral dust aerosols to the scattering and the absorption [*Mallet et al.*, 2008]. Column retrievals of the single scattering albedo from AERONET inversions at M'Bour range from 0.81 to 0.91 at 0.44 μm, with the lower value representing a mixture of biomass burning and mineral dust and the higher value mineral dust. The reasons for the difference between the single scattering albedo for mineral dust from column inversions and in situ measurements is not clear. Differences in sources and chemical compositions [e.g., *Chou et al.*, 2008; *Formenti et al.*, 2008] and problems associated with sampling the coarse mode particles may all be contributing factors.

[49] A simple analysis of the effect of aerosols on the surface radiation balance shows a reduction in the midday solar irradiance of over 25% indicating that aerosols play a significant role in the radiation budget at the surface. Both mineral dust and biomass burning aerosol contribute significantly to the reduction in surface solar irradiance. In Niamey, about 50% of the reduction is due to biomass burning smoke and 50% is due to mineral dust. To the north/south of Niamey, mineral dust/biomass burning aerosol becomes increasingly dominant in its effects on the surface radiation budget. More detailed measurement and modeling studies which diagnose the top of the atmosphere, and atmospheric forcings are presented in a number of studies.

[50] Numerical weather prediction models that concentrate on forecasting the production, transport, and radiative effects of mineral dust reveal that the models do indeed show some significant skill in forecasting dust events several days in advance [*Greed et al.*, 2008; *Milton et al.*, 2008; *Tulet et al.*, 2008]. Current climate models appear to simulate the vertical profiles of aerosols with the biomass burning aerosol being transported at higher altitudes than the mineral dust [*Johnson et al.*, 2008b; *Myhre et al.*, 2008]. This is important because recently *Bellouin et al.* [2008] showed that natural aerosols such as mineral dust must be well simulated in order to accurately assess the direct radiative forcing of anthropogenic aerosols such as those from biomass burning.

[51] Given the objectives described in the introduction, DABEX and AMMA SOP0 can be considered a success, although further studies using this rich set of data are envisaged in the future.

[52] **Acknowledgments.** The authors would like to dedicate this work to Tony Slingo who sadly passed away in October 2008. Tony was an inspiration to so many UK, European, and international scientists. We will remember with great fondness his sharp intellect and wit and the good times shared in Niamey, Niger, while on detachment during 2006. He will be sadly missed. The hard work and dedication of the UK Met Office, FAAM, Direct Flight, and Avalon engineering staff enabled the BAe146 detachment to run smoothly. Boukari, the head of Niamey ATC, is thanked for providing a thoroughly professional service to the aircraft throughout the AMMA SOP0 project. Cyrille Flamant is thanked for comments on an earlier version of the manuscript, and Gerard Devine is thanked for additional analysis and modeling of the dust event of 23/24 January. On the basis of a French initiative, AMMA was built by an international scientific group and is currently funded by a large number of agencies, especially from France, UK, United States, and Africa. It has been the beneficiary of a major financial contribution from the European Community's Sixth Framework Research programme. Detailed information on scientific coordination and funding is available on the AMMA International web site http://www.ammainternational.org.

References

Abel, S., J. M. Haywood, E. J. Highwood, J. Li, and P. R. Buseck (2003), Evolution of biomass burning aerosol properties from an agricultural fire in southern Africa, *Geophys. Res. Lett.*, *30*(15), 1783, doi:10.1029/2003GL017342.

Andreae, M. O., D. Rosenfeld, P. Artaxo, A. A. Costa, G. P. Frank, K. M. Longo, and M. A. F. Silva-Dias (2004), Smoking clouds over the Amazon, *Science*, *303*(5662), 1337–1342, doi:10.1126/science.1092779.

Bellouin, N., O. Boucher, J. M. Haywood, C. Johnson, A. Jones, J. Rae, and S. Woodward (2007), Improved representation of aerosols for HadGEM2, *Tech. Note 73*, Hadley Cent., Exeter, U.K.

Bellouin, N., A. Jones, J. M. Haywood, and S. A. Christopher (2008), Updated estimate of aerosol direct radiative forcing from satellite observations and comparison against the Hadley Centre climate model, *J. Geophys. Res.*, *113*, D10205, doi:10.1029/2007JD009385.

Bond, T. C., D. G. Streets, K. F. Yarber, S. M. Nelson, J.-H. Woo, and Z. Klimont (2004), A technology-based global inventory of black and organic carbon emissions from combustion, *J. Geophys. Res.*, *109*, D14203, doi:10.1029/2003JD003697.

Brindley, H. E. (2007), Estimating the top-of-atmosphere longwave radiative forcing due to Saharan dust from satellite observations over a west African surface site, *Atmos. Sci. Lett.*, *8*(3), 74–79, doi:10.1002/asl.155.

Capes, G., B. Johnson, G. McFiggans, P. I. Williams, J. M. Haywood, and H. Coe (2008), Aging of biomass burning aerosols over West Africa: Aircraft measurements of chemical composition, microphysical properties and emission ratios, *J. Geophys. Res.*, *113*, D00C15, doi:10.1029/2008JD009845.

Chazette, P., J. Sanak, and F. Dulac (2007), New approach for aerosol profiling with a lidar onboard an ultralight Aircraft: Application to the African Monsoon Multidisciplinary Analysis, *Environ. Sci. Technol.*, *41*(24), 8335–8341, doi:10.1021/es070343y.

Chou, C., P. Formenti, M. Maille, P. Ausset, G. Helas, S. Osborne, and M. Harrison (2008), Size distribution, shape and composition of dust aerosols collected during the AMMA SOP0 field campaign in the northeast of Niger, January 2006, *J. Geophys. Res.*, *113*, D00C10, doi:10.1029/2008JD009897.

Christian, H. J., et al. (2003), Global frequency and distribution of lightning as observed from space by the Optical Transient Detector, *J. Geophys. Res.*, *108*(D1), 4005, doi:10.1029/2002JD002347.

Christopher, S. A., P. Gupta, J. Haywood, and G. Greed (2008), Aerosol optical thickness over North Africa: 1. Development of a product for model validation using OMI, MISR, and AERONET, *J. Geophys. Res.*, *113*, D00C04, doi:10.1029/2007JD009446.

Clarke, A. D., et al. (2004), Size distributions and mixtures of dust and black carbon aerosol in Asian outflow: Physiochemistry and optical properties, *J. Geophys. Res.*, *109*, D15S09, doi:10.1029/2003JD004378.

Crosier, J., J. D. Allan, H. Coe, K. N. Bower, P. Formenti, and P. I. Williams (2007), Chemical composition of summertime aerosol in the Po Valley (Italy), northern Adriatic and Black Sea, *Q.J.R. Meteorol. Soc.*, *133*, 61–75, doi:10.1002/jq.88.

Cuesta, J., et al. (2008), Multiplatform observations 1 of the seasonal evolution of the Saharan atmospheric boundary layer in Tamanrasset, Algeria, in the framework the African Monsoon Multidisciplinary Analysis field campaign, *J. Geophys. Res.*, *113*, D00C07, doi:10.1029/2007JD009417.

Derimian, Y., J.-F. Leon, O. Dubovik, I. Chiapello, D. Tanré, A. Sinyuk, F. Auriol, T. Podvin, G. Brogniez, and B. N. Holben (2008), Radiative properties of aerosol mixture observed over M'Bour in Senegal during the dry season 2006 (African Monsoon Multidisciplinary Analysis campaign), *J. Geophys. Res.*, *113*, D00C09, doi:10.1029/2008JD009904.

Dubovik, O., B. N. Holben, T. F. Eck, A. Smirnov, Y. J. Kaufman, M. D. King, D. Tanré, and I. Slutsker (2002), Variability of absorption and optical properties of key aerosol types observed in worldwide locations, *J. Atmos. Sci.*, *59*, 590–608.

Dubovik, O., et al. (2006), Application of spheroid models to account for aerosol particle nonsphericity in remote sensing of desert dust, *J. Geophys. Res.*, *111*, D11208, doi:10.1029/2005JD006619.

Dulac, F., P. Chazette, L. Gomes, B. Chatenet, H. Berger, and J. M. Vinicula dos Santos (2001), A method for aerosol profiling in the lower troposphere with coupled scatter and meteorological rawinsondes and first data from the tropical Atlantic off Sahara, *J. Aerosol Sci.*, *32*, 1069–1086, doi:10.1016/S0021-8502(01)00043-X.

Flamant, C., J.-P. Chaboureau, D. J. Parker, C. M. Taylor, J.-P. Cammas, O. Bock, F. Timouk, and J. Pelon (2007), Airborne observations of the impact of a convective system on the planetary boundary layer thermodynamics and aerosol distribution in the inter-tropical discontinuity region of the West African Monsoon, *Q.J.R. Meteorol. Soc.*, *133*, 1175–1189, doi:10.1002/qj.97.

Formenti, P., et al. (2008), Regional variability of the composition of mineral dust from western Africa: Results from the AMMA SOP0/DABEX and DODO field campaigns, *J. Geophys. Res.*, *113*, D00C13, doi:10.1029/2008JD009903.

Forster, P., et al. (2007), Changes in atmospheric constituents and in radiative forcing, in *Climate Change 2007: The Physical Science Basis. Contribution of Working Group I to the Fourth Assessment Report of the Intergovernmental Panel on Climate Change*, edited by S. Solomon et al., pp. 129–234, Cambridge Univ. Press, Cambridge, U.K.

Greed, G., J. M. Haywood, S. Milton, A. Keil, S. Christopher, P. Gupta, and E. J. Highwood (2008), Aerosol optical depths over North Africa: 2. Modeling and model validation, *J. Geophys. Res.*, *113*, D00C05, doi:10.1029/2007JD009457.

Hastenrath, S., and P. Lamb (1977), Some aspects of circulation and climate over eastern equatorial Atlantic, *Mon. Weather Rev.*, *105*, 1019–1023, doi:10.1175/1520-0493(1977)105<1019:SAOCAC>2.0.CO;2.

Haywood, J. M., and O. Boucher (2000), Estimates of the direct and indirect radiative forcing due to tropospheric aerosols: A review, *Rev. Geophys.*, *38*, 513–543, doi:10.1029/1999RG000078.

Haywood, J. M., P. Francis, S. R. Osborne, M. Glew, N. Loeb, E. Highwood, D. Tanré, G. Myhre, P. Formenti, and E. Hirst (2003a), Radiative properties and direct radiative effect of Saharan dust measured by the C-130 aircraft during SHADE: 1. Solar spectrum, *J. Geophys. Res.*, *108*(D18), 8577, doi:10.1029/2002JD002687.

Haywood, J. M., S. R. Osborne, P. N. Francis, A. Keil, P. Formenti, M. O. Andreae, and P. H. Kaye (2003b), The mean physical and optical properties of regional haze dominated by biomass burning aerosol measured from the C-130 aircraft during SAFARI 2000, *J. Geophys. Res.*, *108*(D13), 8473, doi:10.1029/2002JD002226.

Heese, B., and M. Wiegner (2008), Vertical aerosol profiles from Raman-depolarization lidar observations during the dry season AMMA field campaign, *J. Geophys. Res.*, *113*, D00C11, doi:10.1029/2007JD009487.

Huebert, B. J., et al. (2003), An overview of ACE-Asia: Strategies for quantifying the relationships between Asian aerosols and their climatic impacts, *J. Geophys. Res.*, *108*(D23), 8633, doi:10.1029/2003JD003550.

Johnson, B. T., S. R. Osborne, J. M. Haywood, and M. A. J. Harrison (2008a), Aircraft measurements of biomass burning aerosols over West Africa during DABEX, *J. Geophys. Res.*, *113*, D00C06, doi:10.1029/2007JD009451.

Johnson, B. T., B. Heese, S. A. McFarlane, P. Chazette, A. Jones, and N. Bellouin (2008b), Vertical distribution and radiative effects of mineral dust and biomass burning aerosol over west Africa during DABEX, *J. Geophys. Res.*, *113*, D00C12, doi:10.1029/2008JD009848.

Kaufman, Y. J., Q. Ji, A. M. Thompson, J. F. Gleason, S. A. Christopher, and S.-C. Tsay (1998), Smoke, Clouds, and Radiation-Brazil (SCAR-B) experiment, *J. Geophys. Res.*, *103*(D24), 31,783–31,808, doi:10.1029/98JD02281.

Knippertz, P. (2005), Tropical-extratropical interactions associated with an Atlantic tropical plume and subtropical jet streaks, *Mon. Weather Rev.*, *133*, 2759–2776, doi:10.1175/MWR2999.1.

Lelieveld, J., et al. (2002), Global air pollution crossroads over the Mediterranean, *Science*, *298*(5594), 794–799, doi:10.1126/science.1075457.

Linden, P. F., and J. E. Simpson (1986), Gravity-driven flows in a turbulent fluid, *J. Fluid Mech.*, *172*, 481–497, doi:10.1017/S0022112086001829.

Mallet, M., et al. (2008), Aerosol direct radiative forcing on Djougou (northern Benin) during the African Monsoon Multidisciplinary Analysis dry season experiment (SOP-0), *J. Geophys. Res.*, *113*, D00C01, doi:10.1029/2007JD009419.

Marsham, J. H., D. J. Parker, C. M. Grams, C. M. Taylor, and J. M. Haywood (2008), Uplift of Saharan dust south of the intertropical discontinuity, *J. Geophys. Res.*, *113*, D21102, doi:10.1029/2008JD009844.

McConnell, C. L., E. J. Highwood, H. Coe, P. Formenti, B. Anderson, S. Osborne, S. Nava, K. Desboeufs, G. Chen, and M. A. J. Harrison (2008), Seasonal variations of the physical and optical characteristics of Saharan dust: Results from the Dust Outflow and Deposition to the Ocean (DODO) experiment, *J. Geophys. Res.*, *113*, D14S05, doi:10.1029/2007JD009606.

Miller, M. A., and A. Slingo (2007), The ARM Mobile Facility and its first international deployment: Measuring radiative flux divergence in West Africa, *Bull. Am. Meteorol. Soc.*, *88*, 1229–1244, doi:10.1175/BAMS-88-8-1229.

Milton, S. F., G. Greed, M. Brooks, J. M. Haywood, B. Johnson, R. P. Allan, A. Slingo, and W. M. F. Grey (2008), Modeled and observed atmospheric radiation balance during the West African dry season: Role of mineral dust, biomass burning aerosol, and surface albedo, *J. Geophys. Res.*, *113*, D00C02, doi:10.1029/2007JD009741.

Mishchenko, M. I., L. D. Travis, R. A. Kahn, and R. A. West (1997), Modeling phase functions for dustlike tropospheric aerosols using a shape mixture of randomly oriented polydisperse spheroids, *J. Geophys. Res.*, *102*(D14), 16,831–16,847, doi:10.1029/96JD02110.

Myhre, G., C. R. Hoyle, T. F. Berglen, B. T. Johnson, and J. M. Haywood (2008), Modeling of the solar radiative impact of biomass burning aerosols during the DABEX experiment, *J. Geophys. Res.*, doi:10.1029/2008JD009857, in press.

Normand, C. W. B. (1938), Kinetic energy liberated in an unstable layer, *Q.J.R. Meteorol. Soc.*, *64*, 71–74.

Nwofor, O. K., T. Chidiezie Chineke, and R. T. Pinker (2007), Seasonal characteristics of spectral aerosol optical properties at a sub-Saharan site, *Atmos. Res.*, *85*(1), 38–51, doi:10.1016/j.atmosres.2006.11.002.

Osborne, S. R., B. T. Johnson, J. M. Haywood, A. Baran, M. Harrison, and C. L. McConnell (2008), Physical and optical properties of mineral dust aerosol during the Dust and Biomass-burning Experiment, *J. Geophys. Res.*, *113*, D00C03, doi:10.1029/2007JD009551.

Parker, D. J., R. R. Burton, A. Diongue-Niang, R. J. Ellis, M. Felton, C. M. Taylor, C. D. Thorncroft, P. Bessemoulin, and A. M. Tompkins (2005), The diurnal cycle of the west African monsoon circulation, *Q.J.R. Meteorol. Soc.*, *131*, 2839–2860, doi:10.1256/qj.04.52.

Parker, D. J., et al. (2008), The AMMA radiosonde program and its implications for the future of atmospheric monitoring over Africa, *Bull. Am. Metorol. Soc.*, *89*, 1015–1027.

Pelon, J., M. Mallet, A. Mariscal, P. Goloub, D. Tanré, D. Bou Karam, C. Flamant, J. Haywood, B. Pospichal, and S. Victori (2008), Micro-lidar observations of biomass burning aerosol over Djougou (Benin) during African Monsoon Multidisciplinary Analysis Special Observation Period 0: Dust and Biomass-Burning Experiment, *J. Geophys. Res.*, doi:10.1029/2008JD009976, in press.

Raes, F., T. Bates, F. McGovern, and M. Liedekerke (2000), The 2nd Aerosol Characterisation Experiment (ACE-2), General overview and main results, *Tellus, Ser. B*, *52*, 111–125.

Rajot, J. L., et al. (2008), AMMA dust experiment: An overview of measurements during the dry season special observation period (SOP0) at the Banizoumbou (Niger) supersite, *J. Geophys. Res.*, *113*, D00C14, doi:10.1029/2008JD009906.

Ramanathan, V., et al. (2001), Indian Ocean experiment: An integrated analysis of the climate forcing and effects of the great Indo-Asian haze, *J. Geophys. Res.*, *106*(D22), 28,371–28,398, doi:10.1029/2001JD900133.

Redelsperger, J. L., C. D. Thorncroft, A. Diedhiou, T. Lebel, D. J. Parker, and J. Polcher (2006), African Monsoon Multidisciplinary Analysis: An international research project and field campaign, *Bull. Am. Meteorol. Soc.*, *87*, 1739–1746, doi:10.1175/BAMS-87-12-1739.

Reid, J. S., et al. (2003), Analysis of measurements of Saharan dust by airborne and ground-based remote sensing methods during the Puerto Rico Dust Experiment (PRIDE), *J. Geophys. Res.*, *108*(D19), 8586, doi:10.1029/2002JD002493.

Slingo, A., et al. (2006), Observations of the impact of a major Saharan dust storm on the atmospheric radiation balance, *Geophys. Res. Lett.*, *33*, L24817, doi:10.1029/2006GL027869.

Slingo, A., et al. (2008), Overview of observations from the RADAGAST experiment in Niamey, Niger: Meteorology and thermodynamic variables, *J. Geophys. Res.*, *113*, D00E01, doi:10.1029/2008JD009909.

Swap, R. J., et al. (2002), The Southern African Regional Science Initiative (SAFARI 2000) dry-season field campaign: An overview, *S. Afr. J. Sci.*, *98*, 125–130.

Tanré, D., J. M. Haywood, J. Pelon, J. F. Léon, B. Chatenet, P. Formenti, P. Francis, P. Goloub, E. J. Highwood, and G. Myhre (2003), Measurement and modeling of the Saharan dust radiative impact: Overview of the SaHAran Dust Experiment (SHADE), *J. Geophys. Res.*, *108*(D13), 8574, doi:10.1029/2002JD003273.

Todd, M. C., R. Washington, J. V. Martins, O. Dubovik, G. Lizcano, S. M'Bainayel, and S. Engelstaedter (2007), Mineral dust emission from the Bodélé Depression, northern Chad, during BoDEx 2005, *J. Geophys. Res.*, *112*, D06207, doi:10.1029/2006JD007170.

Tulet, P., M. Mallet, V. Pont, J. Pelon, and A. Boone (2008), The 7–13 March dust storm over West Africa: Generation, transport, and vertical stratification, *J. Geophys. Res.*, *113*, D00C08, doi:10.1029/2008JD009871.

Washington, R., M. C. Todd, S. Engelstaedter, S. Mbainayel, and F. Mitchell (2006), Dust and the low-level circulation over the Bodélé

Depression, Chad: Observations from BoDEx 2005, *J. Geophys. Res.*, *111*, D03201, doi:10.1029/2005JD006502.

Woodward, S. (2001), Modeling the atmospheric life-cycle and radiative impact of mineral dust in the Hadley Centre climate model, *J. Geophys. Res.*, *106*(D16), 18,155–18,166, doi:10.1029/2000JD900795.

N. Bharmal, ESSC, University of Reading, 3 Earley Gate, Whiteknights, Reading RG6 6AL, UK. (n.a.bharmal@reading.ac.uk)

M. Brooks, G. Greed, M. Harrison, J. M. Haywood, B. Johnson, S. Milton, and S. R. Osborne, Met Office, FitzRoy Road, Exeter EX5 1LZ, UK. (malcolm.e.brooks@metoffice.gov.uk; glenn.greed@metoffice.gov.uk; mark.harrison@metoffice.gov.uk; jim.haywood@metoffice.gov.uk; ben.johnson@metoffice.gov.uk; sean.milton@metoffice.gov.uk; simon.osborne@metoffice.gov.uk)

P. Chazette and M. Schulz, CEA, DSM, LSCE, Orme des Merisiers, F-91191 Gif sur Yvette, France. (patrick.chazette@lsce.ipsl.fr; michael.schulz@lsce.ipsl.fr)

C. Chou, K. Desboeufs, P. Formenti, and B. Marticorena, LISA, Université Denis Diderot, CNRS, F-94000 Créteil, France. (chou@lisa.univ-paris12.fr; desboeufs@lisa.univ-paris12.fr; formenti@lisa.univ-paris12.fr; marticorena@lisa.univ-paris12.fr)

S. Christopher, Earth System Science Center, NSTC, University of Alabama, 320 Sparkman Drive, Hunstville, AL 35805-1912, USA. (sundar@nsstc.uah.edu)

H. Coe and G. Capes, School of Earth, Atmospheric and Environmental Sciences, University of Manchester, Simon Building, Oxford Road, Manchester M13 9PL, UK. (gerard.capes@postgrad.manchester.ac.uk; hugh.coe@manchester.ac.uk)

J. Cuesta, Laboratoire de Météorologie Dynamique, Institute Pierre Simon Laplace, Ecole Polytechnique, F-91128 Palaiseau, France. (cuesta@lmd.polytechnique.fr)

Y. Derimian and D. Tanré, Laboratoire d'Optique Atmosphérique, Université des Sciences et Technologies de Lille, CNRS, Bat. P5, F-59655 Villeneuve d'Ascq, France. (derimian@loa.univ-lille1.fr; Didier.Tanre@univ-lille1.fr)

B. Heese, Leibniz Institute for Tropospheric Research, Permoser Strasse 15, D-04318 Leipzig, Germany. (heese@tropos.de)

E. J. Highwood, Department of Meteorology, University of Reading, Reading RG6 6BB, UK. (e.j.highwood@reading.ac.uk)

M. Mallet, Laboratoire d'Aerologie, UPS, CNRS, UMR5560, 14 Avenue Edouard Belin, Toulouse F-31400, France. (Marc.Mallet@aero.obs-mip.fr)

J. Marsham and D. J. Parker, Institute for Climate and Atmospheric Science Environment, School of Earth and Environment, University of Leeds, Leeds LS2 9JT, UK. (j.marsham@see.leeds.ac.uk; d.j.parker@see.leeds.ac.uk)

G. Myhre, Center for International Climate and Environmental Research, P.O. Box 1129, Blindern, N-0318 Oslo, Norway. (gunnar.myhre@cicero.uio.no)

J. Pelon, Service de Aéronomie, IPSL, Université Pierre et Marie Curie, Boite 102, 4 Place Jussieu, F-75252 Paris CEDEX 05, France. (Jacques.pelon@aero.jussieu.fr)

J.-L. Rajot, IRD, UR176, Niamey, Niger. (jeanlouis.rajot@ird.fr)

P. Tulet, CNRM, GAME, Meteo-France, F31057 Toulouse, France. (Pierre.Tulet@meteo.fr)